Translational control in the spinal cord regulates gene expression and pain hypersensitivity in the chronic phase of neuropathic pain

Kevin C. Lister[1], Calvin Wong[1], Sonali Uttam[1], Marc Parisien[1,2,3], Patricia Stecum[1], Nicole Brown[1], Weihua Cai[1], Mehdi Hooshmandi[1], Ning Gu[1], Mehdi Amiri[4], Francis Beaudry[5,6], Seyed Mehdi Jafarnejad[7], Diana Tavares-Ferreira[8], Nikhil Nageshwar Inturi[8], Khadijah Mazhar[8], Hien T. Zhao[9], Bethany Fitzsimmons[9], Christos G. Gkogkas[10], Nahum Sonenberg[4], Theodore J. Price[8], Luda Diatchenko[1,2,3], Yaser Atlasi[7], Jeffrey S. Mogil[1,3,11*] and Arkady Khoutorsky[1,2,3*]

[1]Department of Anesthesia, McGill University, Montreal, QC, Canada

[2]Faculty of Dental Medicine and Oral Health Sciences, McGill University, Montreal, QC, Canada

[3]Alan Edwards Centre for Research on Pain, McGill University, Montreal, QC, Canada

[4]Department of Biochemistry and Goodman Cancer Research Centre, McGill University, Montreal, Canada

[5]Département de biomédecine vétérinaire, Faculté de médecine vétérinaire, Université de Montréal, Saint-Hyacinthe, QC, Canada

[6]Centre de recherche sur le cerveau et l'apprentissage (CIRCA), Université de Montréal, Montréal, Québec, Canada

[7]Patrick G. Johnston Centre for Cancer Research, Queen's University Belfast, Belfast, BT9 7AE, UK.

[8]Department of Neuroscience and Center for Advanced Pain Studies, University of Texas at Dallas, Dallas, 75080

[9]Ionis Pharmaceuticals, Inc., Carlsbad, CA, USA

[10]Biomedical Research Institute, Foundation for Research and Technology-Hellas, University Campus, 45110 Ioannina, Greece

[11]Department of Psychology, Faculty of Science, McGill University, Montreal, QC, Canada

* Correspondence: jeffrey.mogil@mcgill.ca; arkady.khoutorsky@mcgill.ca

Summary

Sensitization of spinal nociceptive circuits plays a crucial role in neuropathic pain. This sensitization depends on new gene expression that is primarily regulated via transcriptional and translational control mechanisms. The relative roles of these mechanisms in regulating gene expression in the clinically relevant chronic phase of neuropathic pain are not well understood. Here, we show that changes in gene expression in the spinal cord during the chronic phase of neuropathic pain are substantially regulated at the translational level. Downregulating spinal translation at the chronic phase alleviated pain hypersensitivity. Cell-type-specific profiling revealed that spinal inhibitory neurons exhibited greater changes in translation after peripheral nerve injury compared to excitatory neurons. Notably, increasing translation selectively in all inhibitory neurons or parvalbumin-positive (PV^+) interneurons, but not excitatory neurons, promoted mechanical pain hypersensitivity. Furthermore, increasing translation in PV^+ neurons decreased their intrinsic excitability and spiking activity, whereas reducing translation in spinal PV^+ neurons prevented the nerve injury-induced decrease in excitability. Thus, translational control mechanisms in the spinal cord, particularly in inhibitory neurons, play a role in mediating neuropathic pain hypersensitivity.

KEYWORDS: mRNA translation, neuropathic pain, spinal cord, parvalbumin interneurons.

Introduction

Peripheral nerve injury can cause neuropathic pain, a chronic pain condition that is debilitating and challenging to treat[1-3]. The development (early) and maintenance (late) phases of neuropathic pain are mediated by structural and functional changes in peripheral and central pain-processing compartments via complex interactions between neuronal and non-neuronal cells[3-6]. The persistence of these changes relies on *de novo* gene expression, which is tightly regulated, primarily via transcriptional and translational control mechanisms. Whereas previous studies have characterized transcriptional[7-11] and translational[12,13] changes in the dorsal root ganglia (DRG) and spinal cord following peripheral nerve injury and have demonstrated their important roles during the early stage of neuropathic pain[12,14], the investigations of these mechanisms in the late maintenance phase are lacking.

Studies in neuronal and non-neuronal cells have revealed a poor correlation between the expression levels of distinct mRNAs and the abundance of their corresponding proteins[15,16]. The regulation of mRNA translation significantly affects the cellular proteome, representing an important mechanism to account for the discordance between mRNA and protein expression[17,18]. Thus, it is

essential to investigate the role of translational control in regulating gene expression and pain hypersensitivity during the clinically relevant late phase of neuropathic pain.

Recent methodological advances enable the investigation of genome-wide transcriptional and translational changes (using ribosome profiling [Ribo-seq][19]), as well as the identification of actively translating mRNAs in specific cell types (using translating ribosome affinity purification [TRAP][20]). Here, we employed Ribo-seq and TRAP techniques to study alterations in gene expression in DRG and spinal cord in the early and late phases of neuropathic pain. We found that both transcriptional and translational mechanisms regulate changes in gene expression in DRG in the early phase (4 days after nerve injury) and the late phase (63 days after nerve injury), as well as in the spinal cord in the early phase. Surprisingly, changes in gene expression in the spinal cord in the late phase of neuropathic pain were predominantly regulated at the translational level. Targeting a key translation initiation factor, eukaryotic translation initiation factor 4E (eIF4E), in the spinal cord provided a long-lasting alleviation of evoked and spontaneous pain during the maintenance phase. Cell-type-specific translational profiling, using metabolic labeling and TRAP, revealed greater nerve injury-induced translational changes in spinal inhibitory neurons than in excitatory neurons. Activating translation in all inhibitory or parvalbumin-positive (PV^+) interneurons, but not excitatory neurons, was sufficient to induce hypersensitivity.

Taken together, this study provides a characterization of translational changes in the early and chronic phases of neuropathic pain and reveals the central role of spinal translational control, predominantly in inhibitory neurons, in the maintenance of pain hypersensitivity.

Results

Translational regulation of gene expression in the spinal cord in the chronic phase of neuropathic pain

To study changes in gene expression at both transcriptional (transcriptome) and translational (translatome) levels, we employed Ribo-seq on DRG and lumbar spinal cord tissue obtained from mice subjected to an experimental assay of peripheral nerve damage-induced (i.e., neuropathic) pain, spared nerve injury (SNI, Fig. 1A)[21], or sham surgery. SNI prominently features mechanical hypersensitivity, which develops within 2-4 days of the nerve injury and persists for many months[22]. L3-L5 DRGs and the ipsilateral dorsal half of the corresponding segment of the lumbar spinal cord (illustrated in a schematic diagram in Fig. 1A) were collected on day 4 (early phase) and day 63 (late phase) post-SNI and processed for Ribo-seq. Ribo-seq allows the identification of mRNA fragments (ribosome footprints [rFPs]) where translating ribosomes are bound. These mRNA fragments thus remain protected from nuclease-mediated

RNase degradation, and thereby reveal the number and location of ribosomes on specific transcripts (Fig. 1B)[19]. Normalization to the corresponding transcript abundance from the parallel mRNA-seq analysis provides a measure of mRNA translation efficiency (TE) on a genome-wide scale. Using this approach, we identified transcriptionally- and translationally-regulated genes in each tissue and time-point (n = 3 biological replicates/condition, 15 mice pooled per replicate). In the DRG, a significant number of transcripts were altered at both transcriptional and translational levels at day 4 post-SNI (Fig. 1C and D; Fig. S1A; datasets are provided in Supplementary Table 1). At day 63 post-SNI, the number of transcriptionally altered mRNAs in the DRG decreased compared to day 4 (Fig. 1C and D; Fig. S1B). In the spinal cord, changes in gene expression were less pronounced and on day 4 post-SNI, a comparable number of differentially transcribed genes and differentially translated genes were identified (Fig. 1D and E; Fig. S1A). Surprisingly, on day 63 post-SNI, changes in gene expression in the spinal cord occurred predominantly at the translational but not transcriptional level (Fig. 1D and E; Fig. S1B). Pathway analysis of translationally regulated genes in the spinal cord on day 63 post-SNI showed changes in processes related to extracellular matrix (ECM) organization and its interaction with cell surface receptors, cell adhesion, and protein turnover (Fig. 1F). Collectively, these results indicate that both transcriptional and translational mechanisms mediate changes in gene expression in the DRG in both the early and late phases of neuropathic pain and in the spinal cord in the early phase. In the late chronic phase, however, changes in gene expression in the spinal cord are largely controlled at the translational level.

Suppression of spinal translation alleviates established pain hypersensitivity

The important role of spinal translation in regulating changes in gene expression in the chronic phase of neuropathic pain prompted us to test whether targeting translation in the spinal cord can alleviate established pain hypersensitivity. Translation initiation and the activity of cap-binding protein eIF4E, which facilitates the recruitment of ribosomes to the mRNA, are rate-limiting steps in protein synthesis[23,24]. eIF4E is a key translation initiation factor regulating pain-related plasticity as it integrates information from two signaling pathways that are activated in neuropathic pain to stimulate mRNA translation and promote pain hypersensitivity: the mechanistic target of rapamycin complex 1 (mTORC1), and mitogen-activated protein kinases (MAPKs), such as ERK and p38[18,25,26] (Fig. 2A). Moreover, previous studies have revealed that a partial reduction in eIF4E expression (e.g. in *Eif4e*$^{+/-}$ mice and in mice treated with eIF4E shRNA) is both well-tolerated and alleviates adverse phenotypes in cancer[27] and autism spectrum disorder (ASD)[28,29] mouse models. To study the role of mRNA translation

in chronic pain hypersensitivity, we used an antisense oligonucleotide (ASO) against mouse *Eif4e* to modulate eIF4E expression. To target eIF4E in the central nervous system but not the DRG, we injected eIF4E-ASO via the intracerebroventricular (i.c.v., 100 mg/kg) route[30], resulting in a ~38% reduction in eIF4E protein expression in the lumbar spinal cord 2 weeks post-injection (Fig. 2B), without changing eIF4E levels in the DRG (Fig. 2C). We first assessed the effect of eIF4E downregulation on established pain hypersensitivity. Injection of eIF4E-ASO at week 6 post-SNI alleviated mechanical pain hypersensitivity in the von Frey test two weeks later (at week 8 post-SNI; the experimental time course is provided in Fig. 2D, von Frey data in Fig. 2E). Reduced hypersensitivity persisted for 4 additional weeks (up to week 12 post-SNI), demonstrating a long-lasting effect following a single eIF4E-ASO administration. eIF4E-ASO also attenuated spontaneous pain, as assessed using the Mouse Grimace Scale (MGS) on week 8 post-SNI (Fig. 2F).

We then studied the effect of downregulating eIF4E during the early development phase of neuropathic pain by administering eIF4E-ASO and control-ASO ten days before the peripheral nerve injury. Surprisingly, we found no alleviation of mechanical hypersensitivity at day 4 post-SNI in eIF4E-ASO-injected mice (the experimental time course is provided in Fig. 2G, von Frey data in Fig. 2H). However, testing at later time-points showed that mice injected with eIF4E-ASO exhibited reduced mechanical pain hypersensitivity at week 2 after the nerve injury (Fig. 2H) and the effect became more pronounced at weeks 4 and 8. The MGS was also reduced in eIF4E-ASO-injected mice at week 4 and 8 post-SNI (Fig. 2I). These results indicate that downregulation of eIF4E in the spinal cord using ASO alleviates pain hypersensitivity in the late but not the acute stages of neuropathic pain.

Cell-type-specific translational profiling after peripheral nerve injury

Ribo-seq provided a comprehensive characterization of translational landscape in DRG and spinal cord tissues during the early and late phase of neuropathic pain. However, this approach does not allow the measurement of gene expression in distinct neuronal subtypes and cannot distinguish between neuronal and non-neuronal cells. To assess protein synthesis in specific neuronal sub-populations, we used fluorescence noncanonical amino acid tagging (FUNCAT)[31,32], focusing on two major neuronal subtypes in the spinal cord, excitatory and inhibitory neurons. In FUNCAT, mice are injected with a noncanonical amino acid, azidohomoalanine (AHA), which is charged onto methionine tRNA and incorporated into newly synthesized proteins (Fig. 3A). Visualization of AHA incorporation using click chemistry and fluorescent labeling provides the measure of *de novo* protein synthesis in spinal cord sections. The specificity of this approach was validated using a protein synthesis inhibitor, anisomycin, that blocked

AHA incorporation in the spinal cord (Fig. 3B). FUNCAT analysis showed that AHA incorporation increased at day 4 and day 60 post-SNI in Pax2^{+} inhibitory neurons (day 4: Fig. 3C; day 60: Fig. 3D), whereas no statistically significant changes were found in excitatory neurons (NeuN^{+} and Pax2^{-}).

Next, we employed the TRAP approach to identify specific mRNAs that are actively translated in excitatory and inhibitory neurons. In TRAP, the eGFP-tagged ribosomal protein, L10a, is expressed in a genetically defined cellular population (via a specific gene promoter), followed by immunoprecipitation of tagged ribosomes with an anti-eGFP antibody and the sequencing of ribosome-bound mRNAs (Fig. 4A). We performed TRAP analysis on two major sub-populations of neurons: a subset of excitatory neurons, defined by Tac1 (using *L10a*-eGFP*; Tac1*^{Cre} mice); and inhibitory neurons, defined by GAD2 (using *L10a*-eGFP*; Gad2*^{Cre} mice). Tac1 is expressed in a subset of excitatory interneurons and projection neurons in the spinal cord that play important roles in processing nociceptive information, as well as driving spinal plasticity and chronic pain-related behaviors[33,34]. GAD2^{+} neurons encompass numerous sub-populations of spinal cord inhibitory neurons that are critical for the development and maintenance of neuropathic pain[35,36]. To this end, *L10a*-eGFP*; Tac1*^{Cre} and *L10a*-eGFP*; Gad2*^{Cre} mice were subjected to SNI or sham surgery (bilaterally), and lumbar dorsal spinal cord tissue was collected at day 4 and 60 after the nerve injury. mRNAs isolated from the immunoprecipitated (IP) and input (IN) samples were sequenced. Expression levels (IP/IN) of excitatory and inhibitory neuronal markers and markers of non-neuronal cells are shown in Figure 4B for *L10a*-eGFP*; Gad2*^{Cre} mice and in Figure 4C for *L10a*-eGFP*; Tac1*^{Cre} mice, demonstrating the specificity of the approach. Changes in ribosome occupancy were found in 126 mRNAs in the early phase and 223 mRNAs in the late phase in GAD2^{+} neurons, and 118 mRNAs in the early phase and 161 in the late phase in Tac1^{+} neurons (IP: Fig. 4D-H, IP/IN datasets are provided in Supplementary Table 1), suggesting higher translational changes at day 60 post-SNI in GAD2^{+} inhibitory neurons compared to Tac1^{+} excitatory neurons. Together, these results establish translational changes in GAD2^{+} and Tac1^{+} neurons in the early and late phases of neuropathic pain, revealing greater changes in inhibitory neurons.

eIF4E-dependent translation in inhibitory neurons promotes pain hypersensitivity

The pronounced upregulation of mRNA translation in inhibitory neurons after peripheral nerve injury prompted us to study its functional role in mediating pain hypersensitivity. mTORC1, a master regulator of mRNA translation, stimulates protein synthesis via phosphorylation of the translational repressor eIF4E-binding proteins (4E-BPs), triggering their dissociation from eIF4E to allow translation initiation (Fig. 5A). Accordingly, ablation of 4E-BPs, which mimics the activation of the mTORC1-eIF4E axis,

stimulates translation. There are three isoforms of 4E-BP (4E-BP1, 4E-BP2, and 4E-BP3), which exhibit similar functions but have different tissue distribution[37]. 4E-BP1 is the main isoform in the pain pathway, as 4E-BP1, but not 4E-BP2 whole-body knockout mice show mechanical pain hypersensitivity[37], while 4E-BP3 expression is very low in the nervous system. To increase translation selectively in inhibitory or excitatory neurons, we generated mice lacking 4E-BP1 in each cell type (confirmation of 4E-BP1 ablation is shown in Fig. S2A-D). Deletion of 4E-BP1 in all inhibitory neurons (*Eif4ebp1*$^{fl/fl}$*; Gad2*^{Cre}) induced mechanical hypersensitivity without affecting heat sensitivity (Fig. 5B). A subpopulation of inhibitory neurons, PV^{+} interneurons, specifically gate mechanical allodynia[38-40]. Peripheral nerve injury induces substantial plasticity in PV neurons, resulting in a decrease in their intrinsic excitability and spiking activity, and the consequent disinhibition of postsynaptic PKCɣ interneurons and engagement of myelinated primary afferents in spinal nociceptive circuits[38-40]. Ablation of 4E-BP1 in PV neurons (*Eif4ebp1*$^{fl/fl}$*;Pv*^{Cre}) induced robust mechanical hypersensitivity, similar to *Eif4ebp1*$^{fl/fl}$*;Gad2*^{Cre} mice (Fig. 5C; no change was found in heat sensitivity). Recording from lumbar spinal cord slices showed that PV neurons lacking 4E-BP1 exhibit reduced excitability, as evident by a decreased firing rate in response to a depolarization pulse (Fig. 5D) and elevated rheobase compared to PV neurons from control mice (Fig. 5E). No change was observed in membrane capacitance (Fig. 5F), resting membrane potential (Fig. 5G), and input resistance (Fig. 5H). To study the role of translation in peripheral nerve injury-induced plasticity in spinal PV neurons, we selectively downregulated eIF4E in PV neurons in the lumbar spinal cord before SNI. To this end, an adeno-associated virus (AAV)-expressing shRNAmir against eIF4E (AAV9-CAG-DIO-eGFP-eIF4E-shRNAmir) was injected into the lumbar dorsal horn parenchyma of *Pv*^{Cre} mice 14 days before the SNI (Fig. 5I shows experimental design, Fig. S2E shows confirmation of reduced eIF4E levels). Recordings from PV neurons in spinal cord slices revealed that downregulation of eIF4E in PV neurons prevented the SNI-induced decrease in intrinsic excitability (Fig. 5J). Whereas PV neurons from control mice (*Pv*^{Cre} mice injected with AAV9-CAG-DIO-eGFP-eIF4E-scrambled) exhibited reduced spiking activity and increased rheobase 4 weeks post-SNI compared to sham animals, PV neurons with reduced eIF4E showed no change in their excitability after nerve injury (Fig. 5J: firing frequency; Fig. 5K: rheobase). No change was found in membrane capacitance (Fig. 5L), resting membrane potential (Fig. 5M), and input resistance (Fig. 5N).

In contrast to the behavioral phenotypes of targeting inhibitory neurons, ablation of 4E-BP1 in a broad population of excitatory Vglut2^{+} neurons (*Eif4ebp1*$^{fl/fl}$*;Vglut2*^{Cre}) (Fig. 6A), as well as in a subpopulation of excitatory neurons, defined by Tac1 (*Eif4ebp1*$^{fl/fl}$*;Tac1*^{Cre}) (Fig. 6B), did not change mechanical thresholds. Together, these results indicate that enhanced translation in inhibitory neurons,

and particularly PV neurons, but not excitatory neurons, play a role in mediating spinal plasticity and mechanical allodynia.

Discussion

Previous studies in animal models of neuropathic pain have largely focused on changes in the transcriptome and were mostly limited to early time points after peripheral nerve injury. The growing realization of the important role of translational control in neuronal plasticity and pain sensitization, as well as the uncovering of distinct mechanisms underlying the development and maintenance phases of neuropathic pain[1,18,41,42], prompted us to study gene expression at both transcriptional and translational levels during early and late time points after peripheral nerve injury. Unexpectedly, we discovered that gene expression during the maintenance phase in the spinal cord is substantially regulated at the level of mRNA translation. Furthermore, we demonstrated that the downregulation of a key translation initiation factor, eIF4E, in the spinal cord leads to a long-lasting alleviation of established pain hypersensitivity.

In the late phase of neuropathic pain, we found both transcriptional and translational changes in gene expression in DRG but markedly greater translational changes in the spinal cord than transcriptional changes. Alterations in the DRG transcriptome are consistent with previous analyses in animal models[43-45] and human DRG tissue from individuals with neuropathic pain, which revealed substantial transcriptional changes[8,9] accompanied by neuronal hyperexcitability[9]. Gene expression datasets from human neuropathic spinal cord tissue are not yet available due to paucity of spinal cord samples from individuals with neuropathic pain.

Altered translation at late time points after nerve injury might be linked to maladaptive spinal plasticity. eIF4E downregulation in the spinal cord alleviated pain hypersensitivity at the late, but not early, time point. Since translation is the predominant gene expression mechanism in the spinal cord at the late stage, it is conceivable that downregulation of eIF4E normalizes the translational landscape, thus correcting maladaptive plasticity underlying spinal hyperexcitability. In the early stage after nerve injury, modifications of existing proteins (e.g. via phosphorylation) and transcriptional changes play significant roles[1,2], rendering suppression of translation less efficient.

In the maintenance phase of neuropathic pain, we observed greater translational changes, using FUNCAT and TRAP, in spinal inhibitory neurons compared to excitatory neurons. Moreover, enhancing 4E-BP1-dependent translation in $GAD2^+$ inhibitory and PV^+ neurons, but not excitatory neurons, induced mechanical hypersensitivity. Increasing translation was also sufficient to decrease the excitability and spiking of spinal PV interneurons, whereas suppression of translation in PV neurons prevented SNI-

induced reduction in their excitability. Spinal disinhibition, induced by peripheral nerve injury, plays a key role in central sensitization. Numerous neuronal and non-neuronal mechanisms contribute to this disinhibition, including: K^+-Cl^- cotransporter (KCC2) downregulation causing elevation of intracellular chloride and the resulting weakening of inhibitory neurotransmission[46,47], preferential removal of inhibitory synapses by microglia[48,49], and the modulation of the extracellular matrix[50]. In addition, peripheral nerve injury induces substantial plasticity in spinal PV neurons, leading to the reduction in their synaptic output as well as intrinsic excitability, thereby resulting in the engagement of myelinated low-threshold mechanoreceptive (LTMR) afferents in spinal nociceptive lamina I circuits[38-40]. The reduced synaptic output of PV neurons post-SNI is mediated by the retinoic acid receptor RARα[40]. Our data demonstrate that the reduction in PV neuron intrinsic excitability and spiking activity are mediated, at least partially, by translational activation. The exact molecular mechanisms underlying this form of plasticity, downstream of translation, remain unknown; however, the identification of translationally altered genes in TRAP analysis might facilitate their discovery.

Previous studies have shown that pharmacological targeting of mTORC1 can alleviate hypersensitivity in animal models of inflammation[18,51-54] and inhibition of mTORC1 shortly before or after nerve injury transiently alleviates pain hypersensitivity[14,18]. These effects could be mediated through the downregulation of translation in DRG neurons, or alternatively, via inhibiting translation-independent functions of mTORC1 such as lipid biogenesis, regulation of mitochondrial functions, and autophagy, which are all implicated in neuropathic pain[55-58]. Targeting eIF4E in the spinal cord via eIF4E-ASO does not affect DRG neurons and specifically inhibits the translational control mechanism, without affecting other functions of mTORC1.

In summary, our study provides a characterization of the translational landscape at early and late time points of neuropathic pain and in a subset of excitatory and inhibitory neurons. We identified the substantial role of spinal translation during the late stage of neuropathic pain, particularly in inhibitory neurons, and revealed that ASO-mediated downregulation of spinal translation provided a long-lasting alleviation of established pain hypersensitivity. These findings enhance our understanding of the cell-type- and phase-specific mechanisms underlying neuropathic pain, raising the possibility for the development of targeted therapeutics.

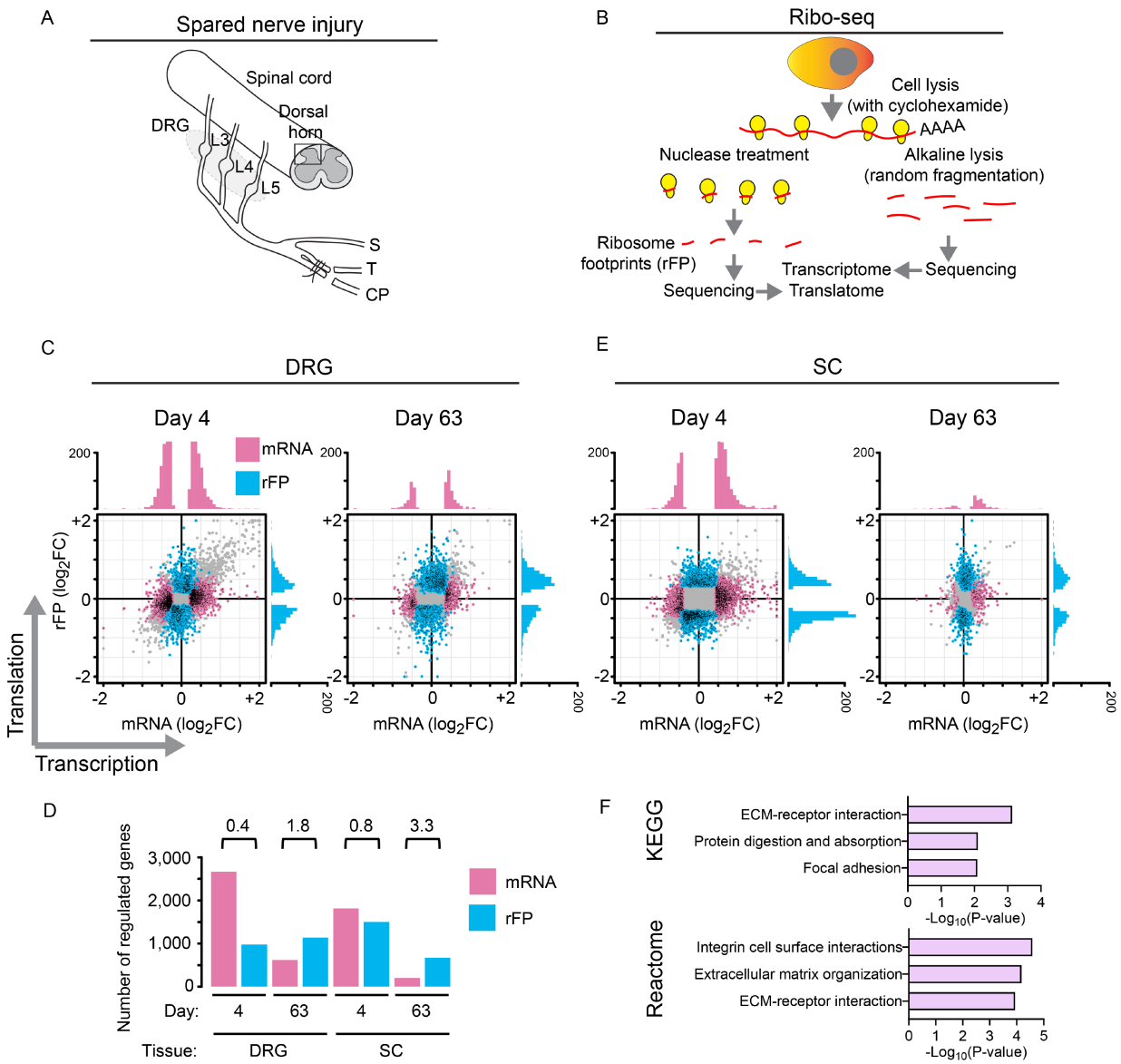

Figure 1. Transcriptional and translational analysis of gene expression using Ribo-seq.

(A) A schematic diagram showing the spared nerve injury (SNI) assay. S: Sural branch, T: Tibial branch and CP: Common peroneal branch. (B) An illustration of the ribosome profiling technique (Ribo-seq). Scatter plot shows ribosomal footprint (rFP) $\log_2$ fold change (FC) as a function of mRNA $\log_2$ fold change for dorsal root ganglia (DRG, C) and spinal cord (SC, E), at day 4 and day 63 post-SNI. Each dot is a gene. Fold change evaluated between SNI and sham conditions. Color coding indicate modality of differential gene expression control, either at the transcriptional level (mRNA, magenta) or at the translational level (rFP, blue). (D) Number of genes showing changes at mRNA and rFP levels across two independent biological replicates. The rFP/mRNA ratio for each condition is shown above the columns. (F) Pathway analyses of translationally regulated genes in the SC at day 63 post-SNI in the KEGG and Reactome databases.

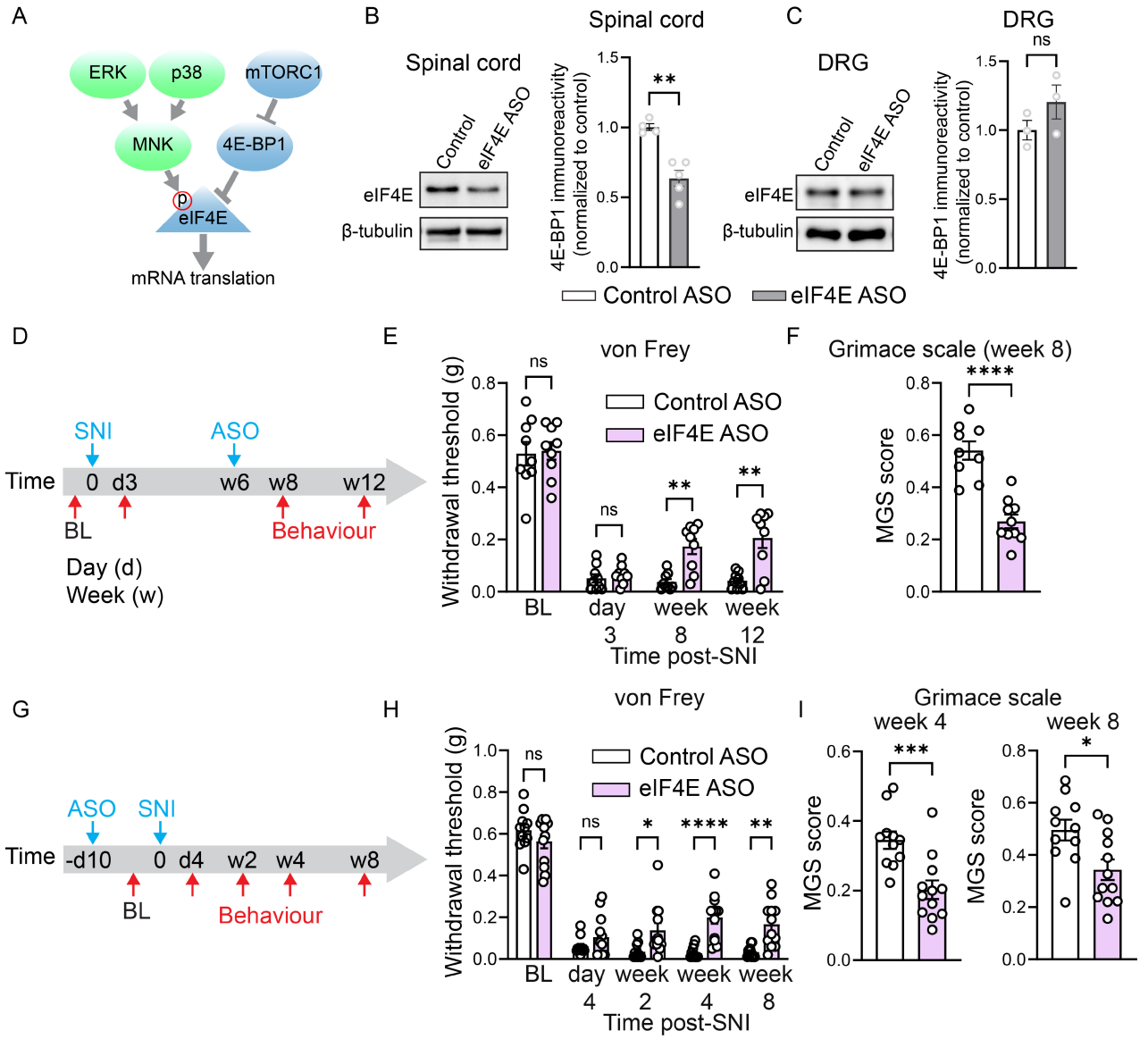

Figure 2. Targeting spinal translation alleviates pain hypersensitivity at the late stage after peripheral nerve injury.

(A) A schematic showing the regulation of eIF4E via mTORC1/4E-BP1 and MAPKs/MNK pathways. eIF4E ASO (i.c.v) reduces eIF4E protein levels in the spinal cord (B) but not DRG (C) two weeks after administration (n = 4/group). (D) Time course of ASO (eIF4E and control) administration after SNI. The effect of ASO on von Frey (E, n = 9/group) and Mouse Grimace Scale (MGS) (F, n = 9/10 mice per group). (G) Time course of ASO administration before SNI and its effect on the von Frey (H, n = 11/12 mice per group) and MGS (I, n = 11/12 mice per group) tests. An unpaired two-tailed *t*-test was used in B, C, F, and I. Two-way ANOVA followed by Tukey's post-hoc comparison was used in E and H. Each data point represents an individual animal. Data are plotted as mean ± s.e.m. $*p < 0.05$, $**p < 0.01$, $***p < 0.001$, $****p < 0.0001$, ns – not significant.

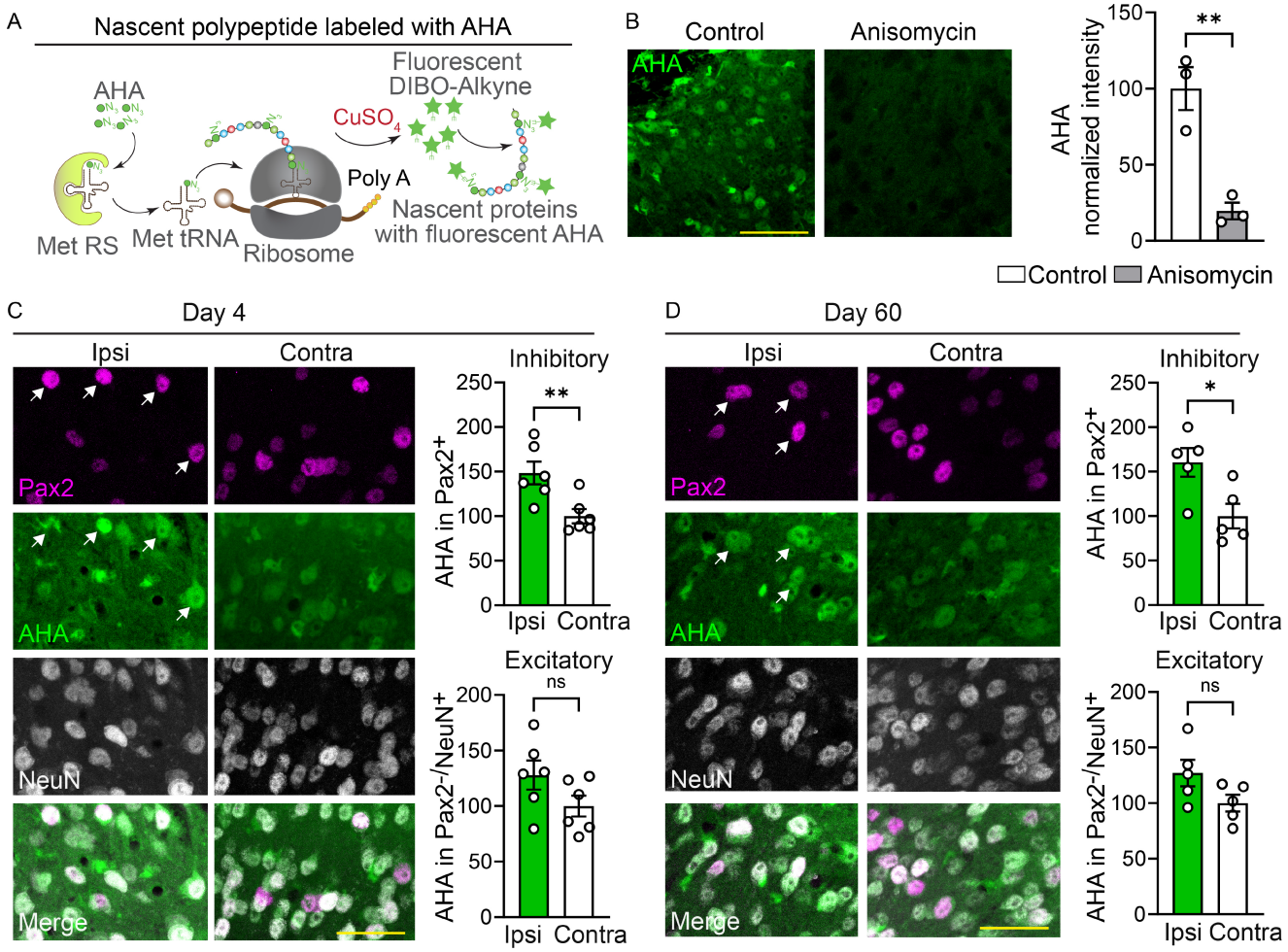

Figure 3. Assessment of protein synthesis using metabolic labeling.

(A) Illustration of protein synthesis assessment using FUNCAT. Anisomycin (100 mg/kg, i.p. injection 1 h before AHA injection) treatment blocked AHA incorporation (n = 3 mice per group), demonstrating the validity of the approach. AHA signal in the superficial spinal cord (laminae I-III) was quantified in inhibitory neurons ($Pax2^+$) and excitatory neurons ($Pax2^-/NeuN^+$) at day 4 (C, n = 6 mice per group) and day 60 (D, n = 5 mice per group) post-SNI. An unpaired two-tailed *t*-test was used. Each data point represents an individual animal. Data are plotted as mean ± s.e.m. $*p < 0.05$, $**p < 0.01$, ns – not significant.

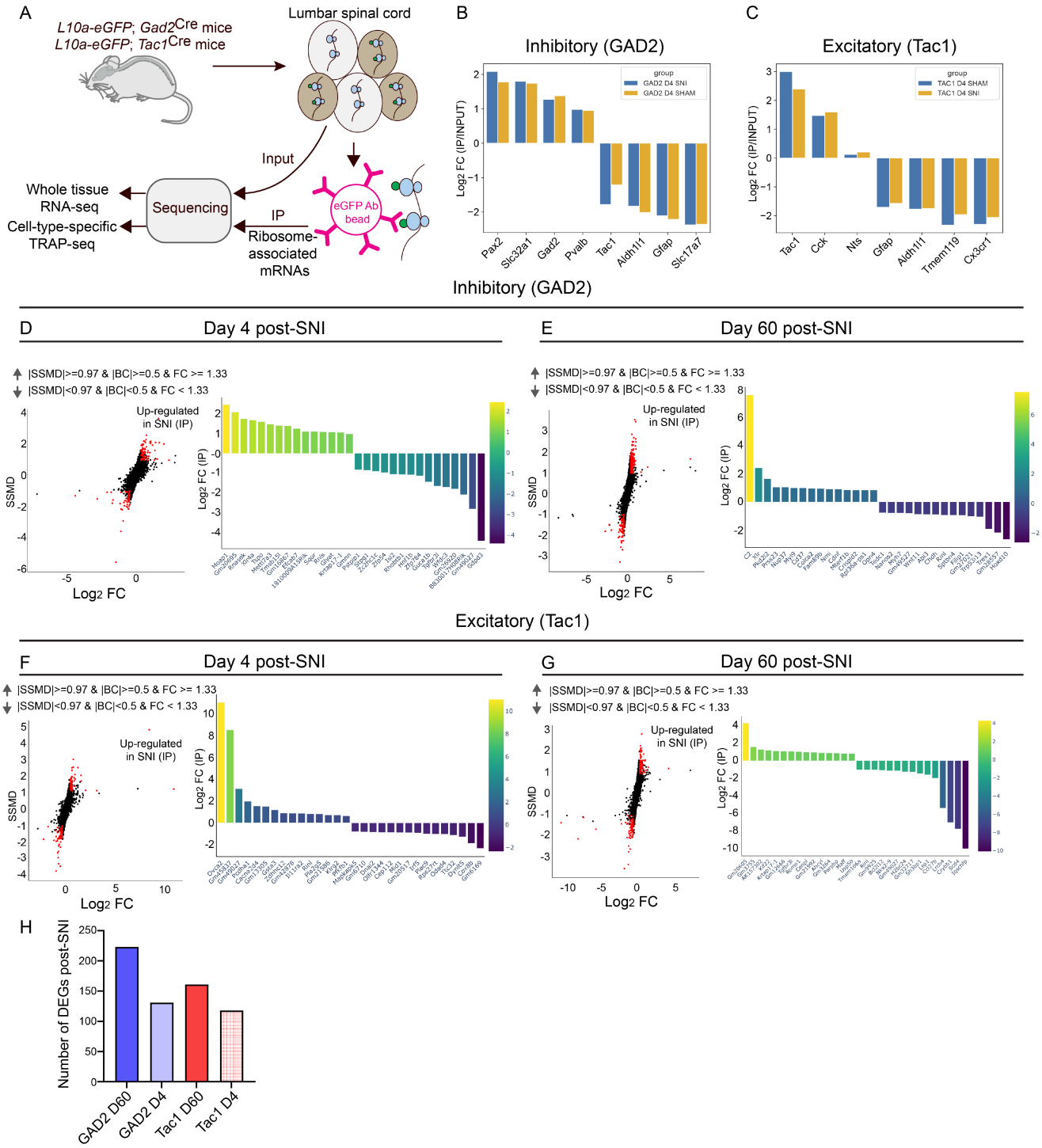

Figure 4. Cell-type-specific profiling of spinal gene expression after peripheral nerve injury.

(A) A schematic describing the TRAP approach to assess gene expression in specific cell types. Confirmation of specificity of IP fractions to inhibitory neurons in *L10a*-eGFP*; Gad2*^{Cre} mouse line (B) and to excitatory neurons in *L10a*-eGFP*; Tac1*^{Cre} mouse line (C). Dual flashlight plots (left) show the strictly standardized mean difference (SSMD) versus $\log_2$ FC for genes in IP samples and panels on the right show the top 15 upregulated and downregulated genes for inhibitory neurons at day 4 (D) and 60

(E), and Tac1^{+} excitatory neurons at day 4 (F) and 60 (G) post-SNI. Positive Log_2 FC indicates increased expression in SNI compared to sham mice. Parameters for defining data as upregulated in SNI are indicated at the top. (H) The number of altered genes in each condition (GAD2 D60: SNI versus sham day 60 in GAD2^{+} neurons; GAD2 D4: SNI versus sham day 4 in GAD2^{+} neurons; Tac1 D60: SNI versus sham day 60 in Tac1^{+} neurons; and Tac1 D4: SNI versus sham day 4 in Tac1^{+} neurons).

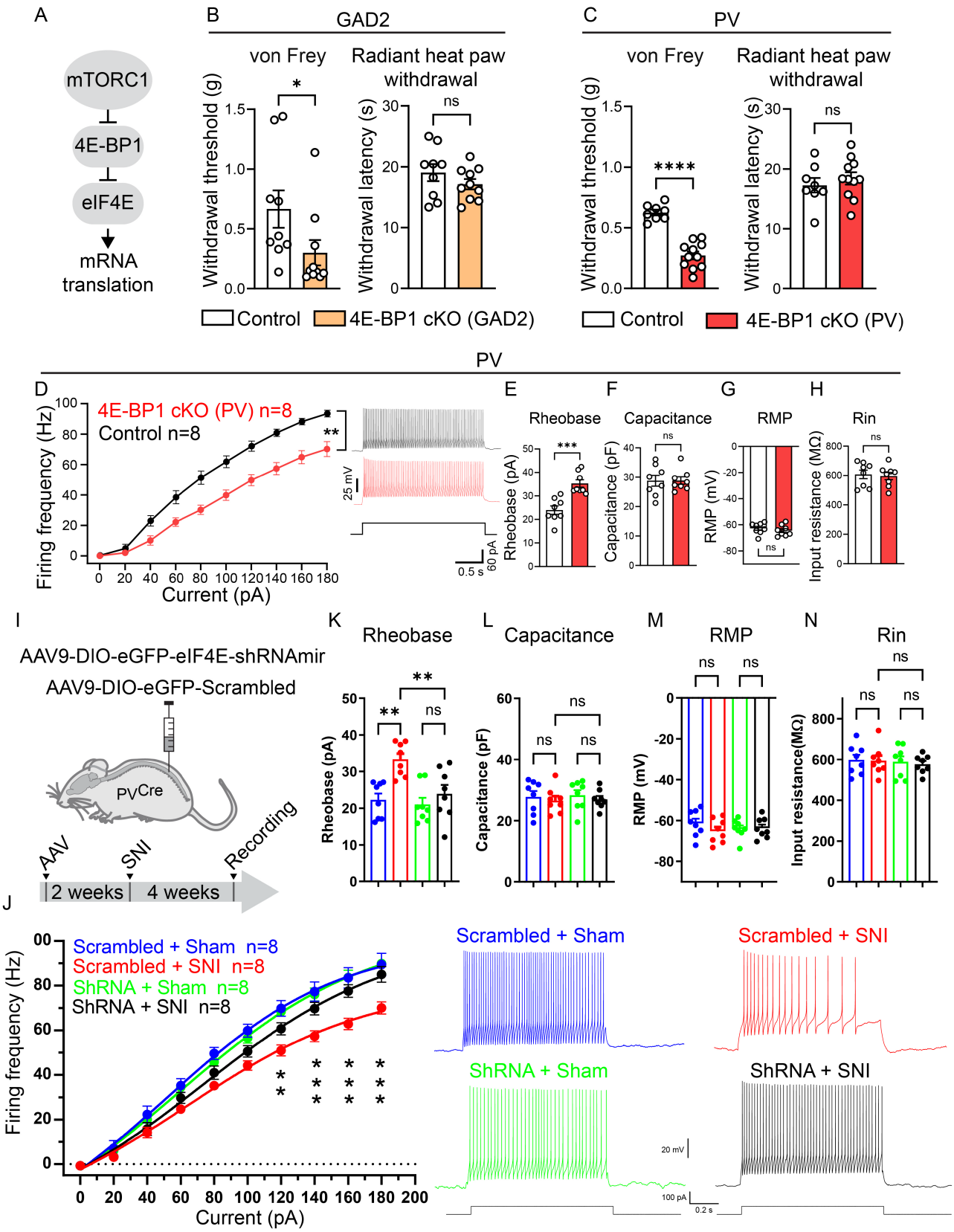

Figure 5. Activation of 4E-BP1-dependent translation in inhibitory neurons promotes plasticity and causes pain hypersensitivity.

(A) A schematic of mTORC1 pathway. Ablation of 4E-BP1 in GAD2 (B, 4E-BP1 cKO: *Eif4ebp1*$^{fl/fl}$*;Gad2*^{Cre}, Control: *Gad2*^{Cre}, n = 9/10) and PV (C, 4E-BP1 cKO: *Eif4ebp1*$^{fl/fl}$*;Pv*^{Cre}, Control: *Pv*^{Cre}, n = 8/11) neurons induces mechanical but not heat hypersensitivity. (C) Recording from PV neurons in spinal cord slices (identified by the expression of L10a-eGFP) shows that the ablation of 4E-BP1 in PV neurons (4E-BP1 cKO: *Eif4ebp1*$^{fl/fl}$*: L10a*-eGFP*: Pv*^{Cre}, Control: *L10a*-eGFP*: Pv*^{Cre}, n = 8/8 mice) induces a decrease in firing frequency (D) and an increase in rheobase (E). No change in membrane capacitance (F), resting membrane potential (RMP, G), and input resistance (Rin, H) were found. AAVs (AAV-CAG-DIO-eGFP-eIF4E-shRNAmir or AAV-CAG-DIO-EGFP-scrambled-shRNAmir) were injected into the parenchyma of the dorsal horn of *Pv*^{Cre} mice (illustration and time course are shown in I, n = 8/group), preventing the SNI-induced decrease in PV neuron firing frequency (J) and elevation of rheobase (K). No changes were found in capacitance (L), RMP (M), and Rin (N). An unpaired two-tailed *t*-test was used in B, C, E-H. Two-way ANOVA followed by Tukey's post-hoc comparison was used in J-N. Each data point represents an individual animal. Data are plotted as mean ± s.e.m. $*p < 0.05$, $**p < 0.01$, $***p < 0.001$, ns – not significant.

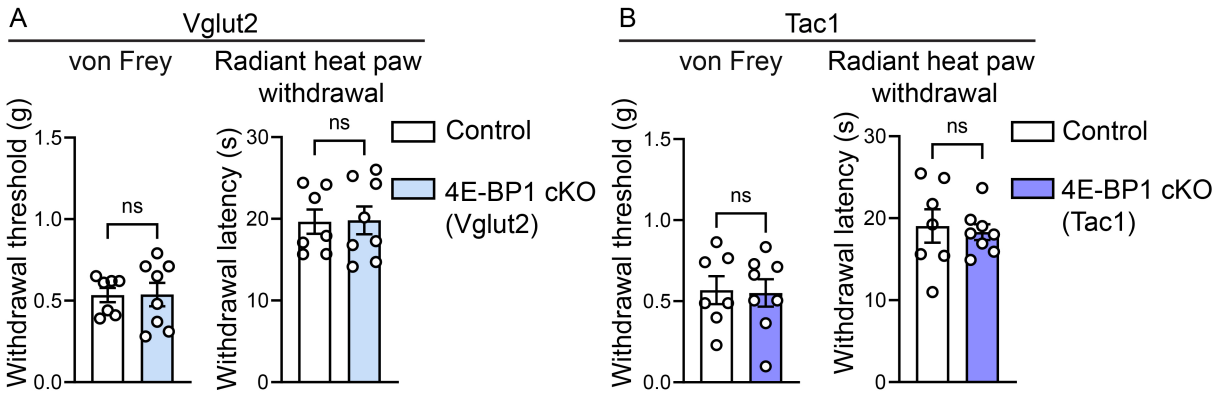

Figure 6. Activation of 4E-BP1-dependent translation in excitatory neurons does not induce pain hypersensitivity.

No changes were observed in mechanical (von Frey) and heat (radiant heat paw-withdrawal) thresholds in mice lacking 4E-BP1 in Vglut2 (A, 4E-BP1 cKO: *Eif4ebp1*$^{fl/fl}$*;Vglut2*^{Cre}, Control: *Vglut2*^{Cre}) and Tac1 neurons (B, 4E-BP1 cKO: *Eif4ebp1*$^{fl/fl}$*;Tac1*^{Cre}, Control: *Tac1*^{Cre}, n = 7/8 mice). An unpaired two-tailed *t*-test. Data are plotted as mean ± s.e.m. ns – not significant.

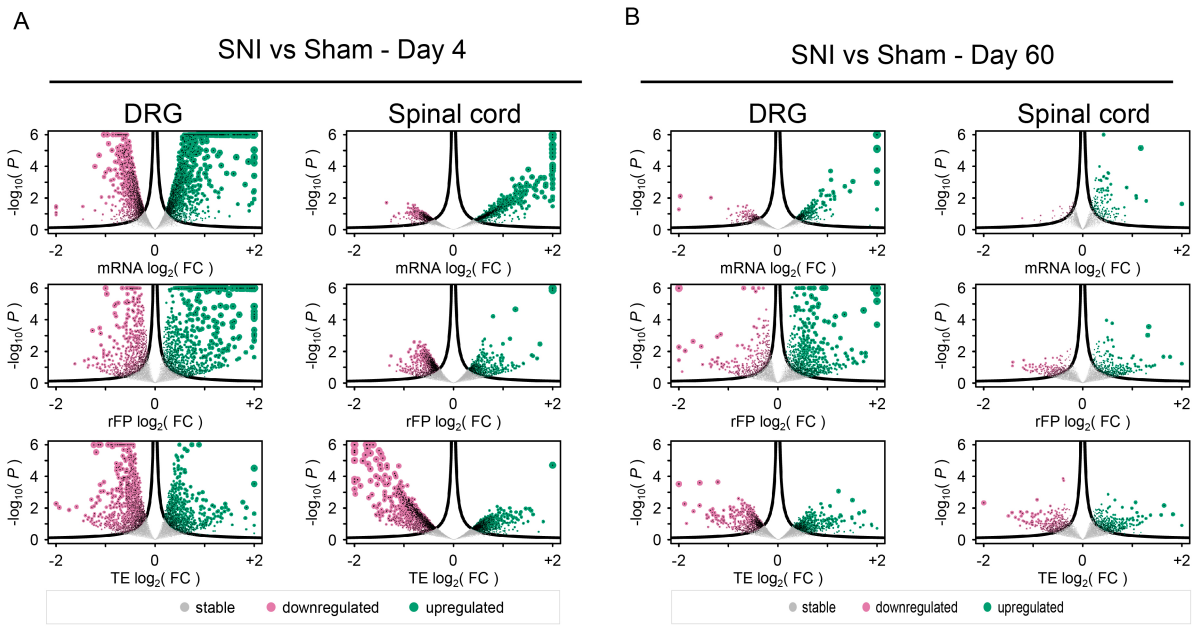

Supplementary Figure 1.

Volcano plots showing changes in mRNA (top), ribosome footprint (rFP, middle), and translational efficiency (TE, bottom) levels in the DRG and SC tissues at day 4 post-SNI (A) and day 63 post-SNI (B). π-values[59] calculated as $\log_2(FC) \cdot -\log_{10}(P)$, given an expression fold-change (FC; X axis) and its associated P-value (P; Y axis). Statistical significance at the alpha=0.2 level; decreased (magenta) or increased fold-change (green) expression in SNI versus sham.

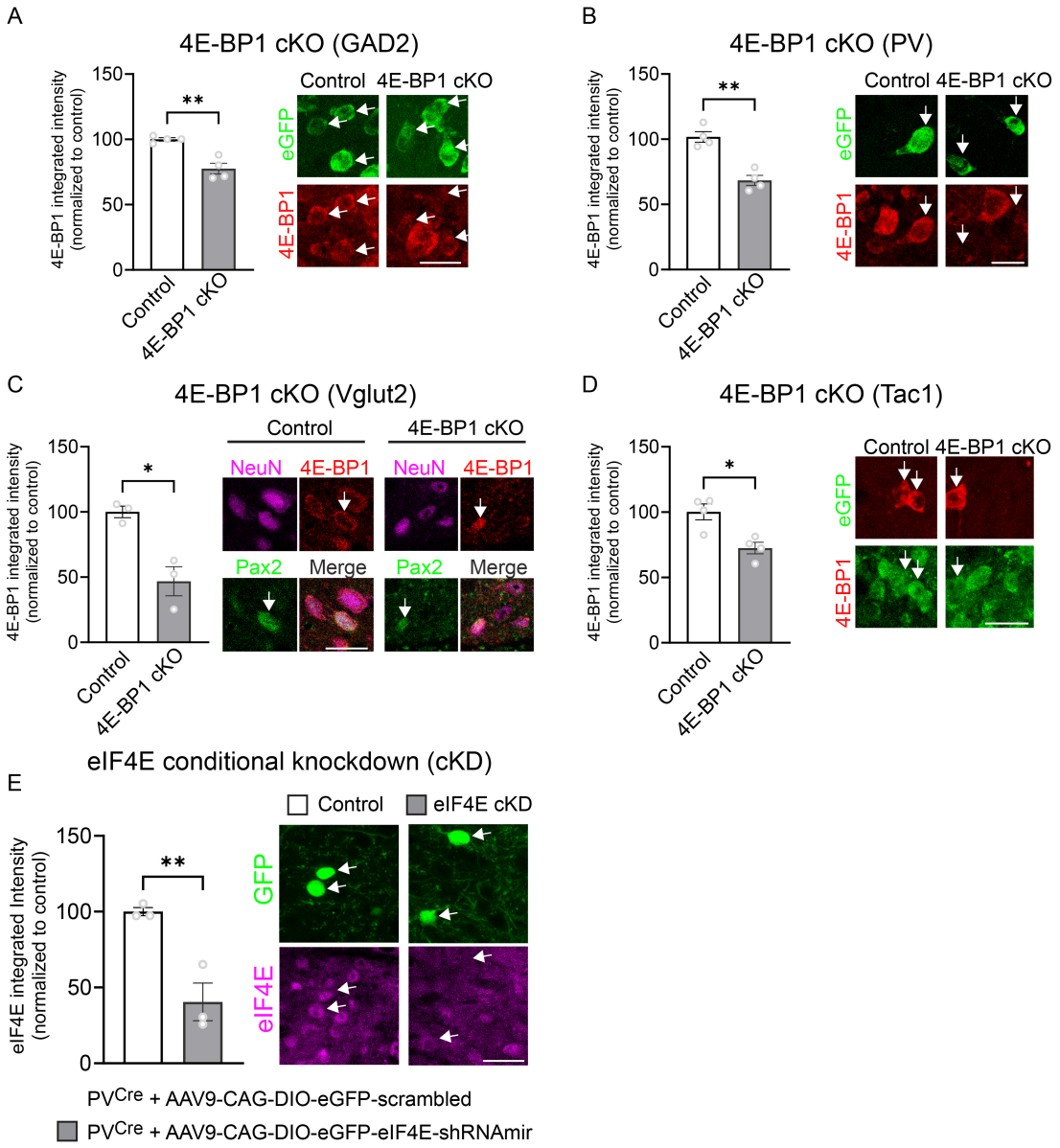

Supplementary Figure 2. Confirmation of 4E-BP1 and eIF4E downregulation.

(A) Lumbar spinal cord tissue from 4E-BP1 cKO GAD2 (*Eif4ebp1*$^{fl/fl}$*: L10a*-eGFP*: Gad2*^{Cre}) and Control (*L10a*-eGFP*: Gad2*^{Cre}) mice was immunostained for 4E-BP1. eGFP expression indicates GAD2^{+} neurons (marked by white arrows). (B) Lumbar spinal cord tissue from 4E-BP1 cKO PV (*Eif4ebp1*$^{fl/fl}$*: L10a*-eGFP*: Pv*^{Cre}) and Control (*L10a*-eGFP*: Pv*^{Cre}) mice were immunostained for 4E-BP1. eGFP expression indicates PV^{+} neurons (marked by white arrows). (C) Lumbar spinal cord tissue from 4E-BP1 cKO Vglut2 (*Eif4ebp1*$^{fl/fl}$*: Vglut2*^{Cre}) and Control (*Pv*^{Cre}) mice was immunostained for 4E-BP1. Excitatory neurons were identified as NeuN^{+}/Pax2^{-} (white arrows mark inhibitory neurons). (D) Lumbar spinal cord tissue from 4E-BP1 cKO Tac1 (*Eif4ebp1*$^{fl/fl}$*: L10a*-eGFP*: Tac1*^{Cre}) and Control (*L10a*-eGFP*: Tac1*^{Cre}) mice was immunostained for 4E-BP1. eGFP expression indicates Tac1^{+} neurons (marked by white arrows). (E) AAVs (AAV9-CAG-DIO-eGFP-eIF4E-shRNAmir and AAV9-CAG-DIO-eGFP-

scrambled) were injected into the lumbar spinal cord of Pv^{Cre} mice and immunohistochemistry against eIF4E was performed 14 days later. Scale bar is 20 µm in all images. An unpaired two-tailed *t*-test was used. Each data point represents an individual animal. Data are plotted as mean ± s.e.m. $*p < 0.05$, $**p < 0.01$.

Materials and methods

Animals and housing conditions

Female C57BL/6 mice were purchased from Charles River Laboratories, Inc. (St. Constant, Quebec, Canada) at 6–7 weeks of age. On arrival at the in-house animal facility, the mice were placed in groups of 5 animals per cage with food and water ad libitum under a 12:12 h light/dark cycle (light period from 07:00-19:00 h) with ambient temperature (22 °C) and humidity maintained at 40%. *Eif4ebp1*$^{fl/fl}$ mice[60] were crossed with *Gad2*^{Cre} (The Jackson Laboratory, stock #010802) to generate *Eif4ebp1*$^{fl/fl}$*;Gad2*^{Cre} animals, *Pv*^{Cre} (Jackson Laboratory, stock #008069) to generate *Eif4ebp1*$^{fl/fl}$*;Pv*^{Cre} animals, *Tac1*^{Cre} (The Jackson Laboratory, stock #021877) to generate *Eif4ebp1*$^{fl/fl}$*;Tac1*^{Cre} animals, and *Vglut2*^{Cre} (The Jackson Laboratory, stock #028863) to generate *Eif4ebp1*$^{fl/fl}$*;Vglut2*^{Cre} animals (corresponding Cre lines were used as controls). *L10a*-eGFP*; Tac1*^{Cre} and *L10a*-eGFP*; Gad2*^{Cre} mice were generated by crossing *L10a*-eGFP mice[61] with the corresponding Cre mouse lines. We also generated *Eif4ebp1*$^{fl/fl}$*: L10a*-eGFP*: Pv*^{Cre}, *Eif4ebp1*$^{fl/fl}$*: L10a*-eGFP*: Gad2*^{Cre}, and *Eif4ebp1*$^{fl/fl}$*: L10a*-eGFP*: Tac1*^{Cre} mice and their controls (no *Eif4ebp1*$^{fl/fl}$) for confirmation of 4E-BP1 ablation experiments and recording from spinal PV neurons (Fig. 5D-H). Sample sizes were determined based on similar previous studies in the field. Female mice were used in Ribo-seq (Fig. 1), TRAP (Fig. 4), FUNCAT (Fig. 3) and electrophysiology experiments. Both sexes (equal number of males and females) were used in all behavioural experiments. All procedures complied with the Canadian Council on Animal Care guidelines and were approved by the McGill University's Downtown Animal Care Committee.

Spared Nerve Injury (SNI)

Mice were anesthetized under 4% isoflurane for induction and 2% for maintenance. The mice were placed on a heated (36-37°C) surgical bed during the surgical procedure. The sciatic nerve was exposed by making an incision in the upper thigh and cutting through the femoris muscle. The tibial and common peroneal branches were ligated with 7.0 silk (Covidien, S-1768K) and a 2–4-mm section of the nerve below the ligation was removed using micro self-opening scissors and forceps, leaving the sural nerve fully intact. The muscle and skin were sutured using 6.0 Vicryl (Ethicon, J489G). All sham surgeries

featured incisions to the thigh and cutting of the femoris muscle, however, the sciatic nerve was left untouched and intact. Mice returned to their cage placed on a heated (36-37 °C) surface for recovery.

Western blotting

Mice were decapitated 2 weeks post-ASO injection. The lumbar section of the spinal cord, and the DRGs, were extracted and immediately homogenized in a homogenization buffer (200 mM HEPES, 50 mM NaCl, 10% Glycerol, 1% Triton X-100, 1mM EDTA, 50 mM NaF, 2 mM Na3VO4, 25 mM β-glycerophosphate, and EDTA-free complete ULTRA tablets (Roche, Indianapolis, IN) before being centrifuged at 14,000 rpm for 15 min at 4 °C to obtain a supernatant. Bradford protein assay was used to measure the protein concentration of the lysates, followed by loading 30 µg of the lysates on a 12 % SDS-PAGE gel, and ran at a constant current (0.03 A/gel). The gel was transferred to a nitrocellulose membrane overnight on ice at 20 mV. The membrane was blocked (5% milk or BSA in TBS-T) for one hour and then incubated in primary antibodies overnight at 4 °C. Afterwards, the membrane was washed three times and incubated in HRP-conjugated secondary antibody at room temperature. The membrane was then washed three times, and an Enhanced Chemiluminescent (ECL) reagent was used to enhance the signal before visualizing it using a ChemiDoc Imaging System (Bio-Rad). Primary antibodies were eIF4E BD (Biosciences, Cat# 610270, 1:1000), and beta-tubulin (Cell Signaling, Cat# 2146S, 1:1000). Secondary antibodies were anti-Rabbit IgG – Horseradish Peroxidase antibody (GE Healthcare, Cat# NA9340 RRID: AB_772191), anti-HRP-conjugated antibody, and sheep anti-Mouse IgG - Horseradish Peroxidase antibody (GE Healthcare, Cat # NA931; RRID: AB_772210).

Fluorescent non-canonical amino acid tagging (FUNCAT)

Female mice, aged 8–10 weeks, were fed a methionine free diet (Envigo RMS Inc., TD.110208) for one week, followed by an intraperitoneal injection of azidohomoalanine (AHA) (100 µg/g body weight, i.p., Click-IT™ AHA [L-Azidohomoalanine], Cat No. C10102, Thermo Fisher Scientific). After 3 h, mice were anesthetized and perfused transcardially with 4% PFA in 0.1 M phosphate buffer, pH 7.4. The L4 and L5 lumbar sections of the spinal cord were extracted and kept at 4 °C in PFA overnight. Tissue was then cut into 30-µm sections and washed three times (10-min increments) in PBST before being blocked overnight in a solution composed of 10% normal goat serum, 0.5% Triton-X100, and 5% sucrose in PBS. Afterwards, click chemistry was performed on the sections overnight in a click buffer, consisting of 200 µM triazole ligand, 400 µM TCEP, 2 µM fluorescent Alexa Fluor 555 alkyne (Alexa Fluor™ 555 Alkyne, Cat No. A20013, Thermo Fisher Scientific), and 200 µM $CuSO_4$ in PBS. The sections were

washed followed by immunohistochemistry (described below). Anisomycin (100 mg/kg) was injected intraperitoneally, and the spinal cord was collected 60 min later.

Immunohistochemistry

Mice were anesthetized and perfused with 4% paraformaldehyde (PFA) in 0.1 M phosphate buffer, pH 7.4, and spinal cords were extracted and left overnight in PFA at 4 °C. Spinal cords were then transversely cut into 30-µm sections followed by three washes (10 min each) using PBS-T. After washing, sections were blocked using a solution consisting of 10% normal donkey and goat serum (NDS/NGS) and 0.2% Triton-X100 in PBS for 1 h. After blocking, tissue was incubated overnight in primary antibodies diluted in PBS. Sections were washed three times in PBS and incubated in the corresponding secondary antibody diluted in PBS for 2 h.

After three washes in PBS, the sections were mounted and imaged using a Zeiss confocal microscope (LSM 880) with 63X/1.40 Oil DIC f/ELYRA objective. Integrated density was measured for FUNCAT signal within $Pax2^{+}$ cells for inhibitory neurons, or $Pax2^{-}/NeuN^{+}$ cells for excitatory neurons in the superficial dorsal horn (laminae I, II and III, defined using a lamina overlay based on NeuN staining) and quantified using ImageJ on maximum intensity projection images. To confirm knockout of 4E-BP1 signal, integrated density of 4E-BP1 signal was measured in $eGFP^{+}$ neurons using *Eif4ebp1*$^{fl/fl}$*: L10a*-eGFP*: Pv*^{Cre}, *Eif4ebp1*$^{fl/fl}$*: L10a*-eGFP*: Gad2*^{Cre}, and *Eif4ebp1*$^{fl/fl}$*: L10a*-eGFP*; Tac1*^{Cre} transgenic mice. Corresponding mouse lines without *Eif4ebp1*$^{fl/fl}$ were used as controls. Background noise was subtracted from the final calculations. Three images were taken from each section (with a total of three sections) for each mouse (n=3–4 mice for each group). For FUNCAT, the integrated intensity of FUNCAT or 4E-BP1 signal in the cytoplasm of at least 25 neurons was quantified using ImageJ on maximum intensity projection images.

Primary antibodies for immunohistochemistry were: NeuN (1:1000, Millipore, MAB377), 4E-BP1 (1:200, #2855S, Cell Signaling and Technology Laboratories), Pax2 (1:500, Novusbio, AF3364) and GFP (1:1000, Abcam, ab13970). Secondary antibodies were Goat anti-rabbit Alexa Fluor 568 (1:500, Thermo Fisher Scientific, A-11011), Donkey anti-goat Alexa Fluor 647 (Thermo Fisher Scientific, A-21447), Goat anti-mouse Alexa Fluor 488 (Thermo Fisher Scientific, A-21042), and Alexa Fluor 555 alkyne (Alexa Fluor™ 555 Alkyne, Cat No. A20013, Thermo Fisher Scientific).

Translating ribosomal affinity purification TRAP

SNI and Sham surgeries were performed on 8–10-week-old female (*L10a*-eGFP*; Tac1*^{Cre} and *L10a*-eGFP*; Gad2*^{Cre}) mice 4 or 60 days prior to tissue extraction. TRAP-sequencing was performed as previously described[13,61]. Mice were decapitated and the lumbar section of the spinal cord was extracted under cold and RNase free conditions and transferred to ice-cold dissection buffer (1X HBSS, 2.5 mM HEPES-NaOH [pH 7.4], 35 mM Glucose, 5 mM $MgCl_2$; 100 µg/mL cycloheximide and 0.2 mg/mL emetine were added just before use). Next, the extracted spinal cord tissues were homogenized in lysis buffer (20 mM HEPES-NaOH [pH 7.4], 12 mM $MgCl_2$ and 150 mM KCl in RNAse free water; 0.5 mM DTT, 1 µL/mL Protease Inhibitors Cocktail [Roche], 100 µg/mL cycloheximide, 20 µg/mL Emetine, 40 U/mL RNasin [Promega] and 2 U/mL TURBO DNase [Invitrogen] were added immediately before use) using Minilys Personal High Power Tissue Homogenizer (Bertin Technologies) on medium speed for 10 s for a total of 8 times with 10-s intervals (incubation on ice) in a cold room at 4 ºC. A post-nuclear fraction was generated from spinal cord homogenates by centrifuging at 2000 x *g* for 5 min at 4 ºC. The supernatant was collected and NP-40 (AG Scientific) and DHPC (Avanti Polar lipids) were added at a final concentration of 1% and incubated on ice for 5 min. Afterward, post-mitochondrial fractions were generated by centrifuging samples at 15,000 x *g* for 10 min. A 200-µL aliquot was taken from the post-mitochondrial fraction and used as the input, and the remaining fraction was incubated overnight with protein washed G-coated Dynabeads (Invitrogen) bound to 50 µg of anti-GFP antibodies (HtzGFP-19F7 and HtzGFP-19C8 antibodies were acquired from Sloan Memorial Kettering Centre) on an end-over-end mixer. On the following day, the beads were washed four times with a high salt buffer (20 mM HEPES-NaOH [pH 7.4], 12 mM $MgCl_2$ and 0.35 M KCl, 1% NP-40 [AG Scientific] in RNAse free water; 100 µg/mL cycloheximide and 0.5 mM DTT were added just before use) to collect the immunoprecipitated fraction (IP). After the removal of the final wash, RNA was extracted by incubating 300 µL of Trizol to the IP fraction and 600 µL to the input fraction for 10 min at room temperature. Equal amounts of ethanol were added to each of the samples before eluting the RNA using a Direct-zol RNA kit (Zymo Research) using manufacturer's protocol. RNA yields were quantified using a NanoDrop Spectrophotometer ND-1000 (NanoDrop Technologies, Inc.) and RNA quality was determined by a 2100 Bioanalyzer (Agilent Technologies).

Library generation and sequencing: Sequencing was performed on immunoprecipitated and corresponding input fractions. Three lumbar sections of the spinal cord were pooled per replicate, with a total of three replicates per group. Groups were labeled as followed: day 4 SNI Tac1 or GAD2, day 4 Sham Tac1 or GAD2, day 60 SNI Tac1 or GAD2, and day 60 Sham Tac1 or GAD2. Total RNA quality

assessment, library generation, library quality check and sequencing were carried out at the Génome Québec (Montreal).

Total RNA was quantified, and its integrity was assessed on a LabChip GXII (PerkinElmer) instrument. rRNA was depleted from 70 ng of total RNA using QIAseq FastSelect (Human/Mouse/Rat 96rxns). cDNA synthesis was achieved with the NEBNext RNA First Strand Synthesis and NEBNext Ultra Directional RNA Second Strand Synthesis Modules (New England BioLabs). The remaining steps of library preparation were performed using and the NEBNext Ultra II DNA Library Prep Kit for Illumina (New England BioLabs). Adapters and PCR primers were purchased from New England BioLabs. Libraries were quantified using the KAPA Library Quantification Kits - Complete kit (Universal) (Kapa Biosystems). The average size fragment was determined using a LabChip GXII (PerkinElmer) instrument.

The libraries were normalized and pooled and then denatured in 0.05 N NaOH and neutralized using HT1 buffer. The pool was loaded at 175 pM on an Illumina NovaSeq S4 lane using Xp protocol as per the manufacturer's recommendations. The run was performed for 2 x100 cycles (paired-end mode). A phiX library was used as a control and mixed with libraries at 1% level. Base calling was performed with RTA v3.4.4 . Program bcl2fastq2 v2.20 was then used to demultiplex samples and generate fastq reads. mRNA library preparation and sequencing were done at Genome Quebec.

TRAP bioinformatics and statistical analysis:

Mapping and TPM quantification

Quality of FASTQ files were checked using FastQC (Babraham Bioinformatics, https://www.bioinformatics.babraham.ac.uk/projects/fastqc/). Phred scores, per-base sequence, and duplication levels were analysed. Reads were soft-clipped (12 bases per read) to ignore adapters and low-quality bases during alignment using STAR v2.7.6 with the GRCm39 mouse reference genome (Gencode release M31, primary assembly)[62]. Reads were also sorted with STAR and then deduplicated with sambamba v0.8.2[63]. StringTie v2.2.1 was used to obtain Transcript Per Million (TPM) values for each gene of all samples[64]. Non-coding and mitochondrial genes were removed and TPM values for coding genes were re-normalized to sum to 1 million before performing downstream analysis.

Order statistics and re-normalization of expression data

Downstream analysis of TRAP datasets was done as previously described[61,65]. Each transcriptome sample (INPUT) had consistently expressed genes identified by calculating percentile ranks for each

coding gene. We identified between 14,763 and 14,812 genes, dependent on condition, that were above the 30th percentile in each INPUT sample. Quantile normalization was performed based on the set of all coding genes. Immunoprecipitation (IP; translatome) analysis was performed on the consistently transcriptome-expressed genes. To identify consistently expressed genes in the translatome samples, the percentile ranks of TPM were calculated for each of the consistently transcriptome-expressed coding genes of each sample. We identified between 13,140–13,191 out of 14,763–14,812 genes, dependent on condition, that are consistently detected in the translatome based on whether their expression was on or above the 10th percentile in each IP sample.

Differential expression (DE) analysis

Differential expression analysis was done as previously described[66]. Log_2-fold change was calculated based upon median TPM values for each transcriptome-expressed and translatome-expressed coding gene in the INPUT and IP samples respectively. Strictly standardized mean difference (SSMD) was used to reveal genes with systematically altered expression percentile ranks between SHAM and SNI mice of the same cell-type and timepoint. SSMD is the difference of means controlled by the variance of the sample measurements. SSMD measured the effect size to control for within-group variability. Differentially expressed genes were determined between Sham and SNI of the same cell-type and timepoint by calculating the Bhattacharyya distance[67]. This measure is used to calculate the amount of overlap in the area under the curve of the two sample distributions (corresponding to each group). BD compares distribution of gene relative to abundance (in TPMs). The Bhattacharyya coefficient BC(Q)i ranges between 0 (for totally non-overlapping distributions) and 1 (for completely identical distributions) and is derived from the Bhattacharyya distance. In our analysis, we used a modified form of the Bhattacharyya coefficient that ranges between 0 (for completely identical distributions) and +1 or -1 (for totally non-overlapping distributions, sign defined by the log-fold change value). DE genes were identified if the absolute value of SSMD was higher or equal to 0.97, the absolute value of BC was higher or equal to 0.5 and fold change higher or equal to 1.33. Coding for bioinformatics analysis and data visualization was done in Python (version 3.7 with Anaconda distribution).

Behavioral pain studies

von Frey

Mice were habituated for 1 h in individual transparent Plexiglas cubicles (5 cm x 8.5 cm x 6 cm) placed on a perforated steel floor. Mice were then tested by applying calibrated nylon monofilaments

perpendicular to the surface of the hind paw for three seconds. Withdrawal of the mouse's foot before the monofilament buckled was considered a positive response. The up-down method of Dixon was used to estimate the 50% withdrawal threshold (average of two measurements separated by at least 30 min)[68].

Radiant heat paw-withdrawal (Hargreaves') assay

Mice were habituated for 1 h in individual transparent Plexiglas cubicles (5 cm x 8.5 cm x 6 cm) placed on a transparent glass floor. During testing, a high-intensity light source was applied to the surface of the hind paw. Intensity was set at 20% (of the maximum) using the IITC model 390. Latency of the hind paw withdrawal was measured. The cut-off for a response was 40 s. Hind paws were measured twice separated by at least 30 min.

Mouse Grimace Scale (MGS)

The Mouse Grimace Scale was adopted from a previous publication[69]. Mice were habituated in custom-made Plexiglas cubicles (5.3 × 8.5 × 3.6 cm) for 1 h. After habituation, mice were recorded (Sony Digital Camcorder HDR-PJ430V) for 1 h. One photo was chosen from every 3-min period for a total of 20 pictures. These pictures were then randomized, and the coder was blinded to the groups before they were analyzed to give each mouse their mean score. Scoring was based off five facial features (action units) including: orbital tightening, nose bulge, cheek bulge, ear position, and whisker change. Scores ranged from 0 to 2, with 0 being no evidence of the action unit present, 1 moderate evidence of the action unit and 2 obvious evidence of the action unit. The final MGS score was given to each mouse based upon averaging the intensity ratings for all five action units.

I.c.v. stereotaxic injection

Mice were deeply anesthetized (induced with 5% isoflurane and maintained on 2% isoflurane) and their head was secured using ear bars in a stereotaxic frame (Kopf). The head was shaved, and an incision was made to expose the skull. Aiming occurred via coordinates relative to bregma (anterior/posterior (AP): -0.5 mm, medial/lateral (ML): 1 mm, and dorsal/ventral (DV): -2.2 mm), and the skull was drilled for injection of the ASO into the lateral ventricles (i.c.v.). Five µL of eIF4E ASO or scrambled ASO was injected using a 10-µL Hamilton microsyringe mounted on a perfusion pump. The perfusion rate was set to 0.5 µL/min, and the needle stayed in place for an additional 5 min to prevent leakage. The timeline of ASO administration, SNI, and behavioral testing is shown in Fig. 2.

eIF4E antisense oligonucleotide

eIF4E ASO targeting mouse *EIf4e* mRNA and Control scrambled ASO were developed and synthesized by Ionis Pharmaceuticals, see Supplementary Table 2 for sequences. Each ASO consists of 5 nucleotides on the 5' and 3' ends of the ASO with a 2'-*O*-methoxyethyl (MOE) modification, and a central 10-base DNA 'gap'. ASO were diluted in phosphate-buffered saline (PBS) to a concentration of 100 mg/ml and were delivered i.c.v. at a single dose of 100 mg/kg.

Intraspinal AAV injections

Eight–10-week-old Pv^{Cre} mice were injected with AAV-CAG-DIO-eGFP-eIF4E-shRNAmir or AAV-CAG-DIO-EGFP-scrambled-shRNAmir using a minimally invasive (non-laminectomy) technique. Mice were deeply anesthetized (induced with 5% isoflurane and maintained on 2% isoflurane) and steel clamps were attached to the vertebral column. An incision was made in the skin and muscle at T12–L3, removing the muscle from the space between the T13 and L1 vertebrae. A glass electrode was inserted 250 µm into the spinal dorsal horn. A total of 500 nL of AAV-shRNA was injected over a 10-min period (David Kopf instruments, 99236B) followed by suturing of the skin using 6-0 Vicryl silk (Ethicon, J489G).

AAV9-shRNAmir cloning and preparation

The microRNA-adapted short hairpin RNAs (shRNAmir) packaged in adeno-associated virus (AAV9-CAG-DIO-eGFP-eIF4E-shRNAmir and AAV9-CAG-DIO-eGFP-scrambled-shRNAmir) were prepared by Vector Biolabs. The validated sequence targeting mouse eIF4E was: TCCAGTTGTCTTAATTTAAGTCAGTCAGTGGCCAAAACTTAAATTACTAGACAACTGGACAG, and the scrambled sequence used as a control was: GAAATGTACTGCGCGTGGAGACGTTTTGGCCACTGACTGACGTCTCCACGCAGTACATTTCAG.

Electrophysiology

Tissue preparation

Six–8-week-old mice were anesthetized with 200 mg/kg tribromoethanol (Avertin, i.p.) and cardiac perfused with 4 °C NMDG-ACSF solution containing (in mM): 92 NMDG, 2.5 KCl, 1.2 NaH_2PO_4, 30 $NaHCO_3$, 20 HEPES, 25 Glucose, 5 Sodium Ascorbate, 2 thiourea, 3 Sodium Pyruvate, 10 $MgSO_4$, 0.5 $CaCl_2$ (pH = 7.3–7.4, 300–310 mOsm). Following the cardiac perfusion, the vertebral column was rapidly

removed and placed in the same oxygenated NMDG-ACSF solution described above. The vertebrae were removed with microforceps and microscissors, under a Zeiss Stemi 305 stereo microscopes, and the dorsal/ventral roots were clipped close to the dorsal root ganglia. The spinal cord of the lumbar region was carefully peeled from the dura matter and superfluous roots and glued to a 2% agar block with the dorsal side up, and then embedded in 3% low melting point agarose. Transverse parasagittal slices (250-µm thick) were made using a Vibratome (Leica VT1200). Slices were incubated at room temperature for 30–45 min in oxygenated recovery solution containing (in mM): 92 NaCl, 2.5 KCl, 1.2 NaH_2PO_4, 30 $NaHCO_3$, 20 HEPES, 25 Glucose, 5 Sodium Ascorbate, 2 thiourea, 3 Sodium Pyruvate, 2 $MgSO_4$, 2 $CaCl_2$ (pH = 7.3–7.4, 300–310 mOsm).

Whole-Cell Recordings

During recording, the spinal cord preparation was kept submerged and perfused with ACSF containing (mM): 125 NaCl, 25 $NaHCO_3$, 1.25 KCl, 1.25 KH_2PO_4, 1.5 $MgCl_2$, 1.5 $CaCl_2$, and 16 glucose and saturated with 95% O_2-5% CO_2, the temperature was kept constant (within ± 0.5 °C), at 30 °C.

Fluorescent-labelled PV neurons at the lamina II-III in the dorsal region of the spinal cord slices were visually identified under the fluorescent microscope (Zeiss axiocam 506). To measure the intrinsic membrane properties and neuronal excitability, whole-cell recordings were performed in current-clamp mode with an increment step of 20 pA (0 – 180 pA), 1-2 second current injections. The patch pipettes were filled with intracellular solution containing (in mM): 140 K-gluconate, 2.5 $MgCl_2$, 10 HEPES, 2 Na_2-ATP, 0.5 Na_2-GTP and 0.5 EGTA (pH 7.3, 295–305 mOsm), and recordings were excluded if the RMP was more positive than −50 mV or series resistance was >25 MΩ.

The data were acquired with pCLAMP 11.0 (Molecular Devices) at a sampling rate of 10-20 kHz and were measured and plotted with pCLAMP 11.0 and GraphPad prism 9.0. Results are reported as mean ± SEM. Statistical analysis of the data was performed using unpaired t-test or one-way ANOVA, followed by Tukey's multiple comparison test. Statistical significance was set at $p < 0.05$.

Ribo-seq

Tissue extraction. On day 4 and day 63 post-SNI or sham surgery, mice were euthanized by isoflurane anesthesia followed by decapitation. Immediately after, the mouse was held vertically, with the rostral end facing down allowing blood to drain from the trunk for about 15–20 s. Then the mouse body was promptly placed and secured on a bed of dry ice using duct tape. The spinal column was carefully cut open to expose the spinal cord and the DRGs, which were doused with RNA*later* (Invitrogen, AM7020).

The lumbar DRGs were extracted from the L3, L4 and L5 vertebrae levels and the corresponding section of the spinal cord was extracted from the T12, T13, and L1 vertebrae levels. The extracted tissues were quickly placed in pre-chilled, RNase-free microcentrifuge tubes (Ambion) and snap frozen by submerging the tubes in liquid nitrogen for a few seconds. The tubes were then stored in a -80 °C freezer until tissue from all animals was collected. Tissue from 15 animals was pooled for each ribosome footprinting (Ribo-seq) replicate.

Ribosome footprinting and RNA-Seq. All consumables and solutions used were certified RNase free by the manufacturer. Bench-top, pipettes, centrifuge rotors, gel tanks, glass Dounce Homogenizers were cleaned with RNaseZap (Invitrogen, AM9780) as per manufacturer's instructions.

Tissue homogenization. Tissue homogenization, RNA and footprint extraction, and library preparation were carried out according to the protocol described by Ingolia et al.,[19] with minor modifications as outlined in Uttam et al.[12].

Briefly, frozen tissue (DRGs or spinal cord, pooled from 15 animals per replicate) was homogenized in 800 µl lysis buffer using pre-chilled 2-ml glass Dounce Homogenizers, performing 30 strokes each with pestle A followed by pestle B. The tissue lysate was collected in a microcentrifuge tube and centrifuged at 16,000 x *g* for 15 min at 4 °C. The total crude RNA content in the supernatant was determined using a NanoDrop1000. A fraction of tissue lysate containing 100 µg total crude RNA was reserved for mRNA-Seq and the remaining was used for ribosome footprinting.

Nuclease footprinting. It was ensured that one complete set of replicates had the same amount of crude total RNA to start with. The RNase I treatment was carried out as described by Ingolia et al.[19] for 45 min at 4 °C using 5 µl of RNase I (Ambion, AM2295) per 250 µg of crude total RNA and quenched by adding 20 µl of SUPERase-In (Ambion, AM2694) per 5µl of RNase I used.

Recovery of ribosome-associated footprints. Ribosome-associated footprints were pelleted by ultra-centrifuging the RNAse I digestion mix (final volume 540 µL) layered on top of a 660 µL sucrose cushion at 71,000 rpm at 4 °C in a Beckman Coulter TLA-120 rotor. The ribosomal pellet was resuspended in 600 µl of 10 mM Tris pH 7 (prepared from 1 M Tris pH 7, Ambion) and stored at –80 °C until all samples for each tissue type were processed until this step.

RNA was purified from the resuspended ribosomal pellet using the Hot-Phenol RNA Extraction method and precipitated with isopropanol. For the Hot-Phenol RNA extraction, the resuspended ribosomal pellet was brought to a final volume of 700 µl with 10 mM Tris pH 7 and supplemented with 40 µl of 20% SDS followed by heated incubation at 65 °C for 1 min at 1400 rpm in a thermomixer. The heated sample-SDS mix was equally split into two microcentrifuge tubes, containing hot acidic phenol

(heated to 65 °C) and incubated at 65 °C, 1400 rpm for 5 min in the thermomixer. Subsequently, the tubes were chilled on ice for 5 min and then centrifuged at 2000 x *g* for 3 min at 4 °C to obtain a top aqueous phase, which was promptly collected in a fresh tube. Seven hundred µl of acidic phenol was added to the aqueous phase and incubated at 25 °C, 14000 rpm in a thermomixer followed by centrifugation to again obtain the top aqueous phase. The top aqueous phase was promptly collected in a fresh tube, to which 600 µl of chloroform was added and mixed by vortexing for 1 min at room temperature. The tubes were then centrifuged to recover the top aqueous phase which was transferred in a fresh tube. The volume of the aqueous phase was estimated using a pipette and 1/9th volume of 3M sodium acetate pH 5.5 (to a final concentration of at least 0.3 M sodium acetate) and 2 µl of 15 mg/ml Glycoblue were added. The tube was vortexed briefly and 1 volume of pre-chilled isopropanol was added followed by overnight storage at -80 °C overnight to aid precipitation. The next morning, the tubes were centrifuged at 20,000 x *g* at 4 °C for 30 min to pellet the precipitated RNA. The supernatant was discarded, and the pellet was washed with 750 µl of ice-cold 80% ethanol, followed by centrifugation at 20,000 x *g* at 4 °C for 5 min. The supernatant was discarded, and the pellet was air dried for up to 5 min before resuspending in 21 µl of 10 mM Tris, pH 7. One µl of the purified RNA was used to assess the RNA concentration on NanoDrop1000.

Purification of footprint fragments and dephosphorylation. Purification of footprint fragments from the ribosome-associated footprint complex and subsequent dephosphorylation was carried out as described in steps 18 to 29 of ref.[19]. In step 25, we selected Rapid Gel Extraction method to extract RNA from polyacrylamide gels. The resultant RNA pellet (dephosphorylated footprints) was resuspended in 9 µl of 10 mM Tris pH7. One µl of the RNA was used to assess the size and concentration of the footprints obtained on the Agilent Bioanalyzer using a Small RNA Bioanalyzer Kit and manufacturer's protocol.

rRNA depletion. Half of the obtained dephosphorylated footprint RNA was processed further for rRNA depletion using Ribo-Zero Gold rRNA Removal Kit (Human/Mouse/Rat) (Illumina, MRZG12324). For each reaction, 90 µl of magnetic beads were transferred to a RNase-free tube and washed two times (1 min each) with an equal volume of RNase-Free water (Ambion, 4387936) using a magnetic stand and resuspended in 35 µl of resuspension solution. To 4 µl of dephosphorylated RNA samples, 12 µl of RNase-free water, 2 µl of Ribo-Zero Reaction Buffer, and 2 µl of Ribo-Zero rRNA Removal Solution was added, mixed by pipetting and incubated at 68 °C for 10 min, followed by a 5-min incubation at room temperature. The treated RNA samples were then transferred to a 1.5-ml microcentrifuge tube containing 35 µl of washed magnetic beads and immediately mixed by pipetting at least 10 times followed by vortexing the tube for 10 s at medium setting. The treated RNA sample and beads mix were

incubated at room temperature for 5 min, after which the tubes were vortexed for 10 s at medium speed and incubated at 50 °C for 5 min. Following this incubation, the tubes were immediately placed on a magnetic stand for at least 1 min and the supernatant was collected in a fresh 1.5-ml microcentrifuge tube. The rRNA depleted samples were purified by adding 100 µl of RNase-free water, 18 µl of 3 M sodium acetate (Ambion), and 2 µl of 10 mg/ml glycogen, vortexed briefly followed by an addition of 600 µl of ice-cold isopropanol and incubated at -80 °C overnight. On the following day, the precipitated RNA was pelleted and purified as described above, and the rRNA-depleted dephosphorylated footprint sample was dissolved in 10 µl of 10 mM Tris, pH 7.

Library preparation from rRNA-depleted dephosphorylated footprint samples. The subsequent steps of linker ligation, reverse transcription and circularization were carried out according to steps 30 to 46, and the PCR amplification and barcode addition steps were carried out as per steps 55 to 64 in the protocol by Ingolia et al.[19] The resulting libraries were referred to as 'footprint libraries'.

Library preparation for mRNA fraction. Total RNA was extracted from the tissue lysate reserved for mRNA sequencing using the hot-phenol method as described above. The extracted total RNA was submitted to Génome Québec (Montreal) for quality assessment and library preparation using the NEB mRNA stranded Library preparation service. The libraries thus generated are referred to as 'mRNA libraries'.

Sequencing and Analysis. Both the rFP and mRNA libraries were sequenced at an aimed sequencing depth of 50 million single-ended reads per sample on the Illumina HiSeq4000 or HiSeq2500 platforms. Demultiplexed sequencing data were provided by Génome Québec (Montreal) as .bam files.

Bioinformatic Analysis for Ribosome footprinting data. The adapter sequence was identified using DREME-MEME Suite[70] and trimmed from all the rFP reads using Trimmomatic[71]. Next, using Bowtie[71], the rFP and mRNA reads were mapped to mouse reference genome mm10. Read counts for the uniquely mapped reads were generated and differentially translated genes were identified using the Xtail pipeline as described by Xiao et al[72]. Transcriptionally- and translationally-regulated genes were identified by Xtail using default settings. Pathway analysis was carried out using Enrichr[73], using the Kyoto Encyclopedia of Genes and Genomes (KEGG)[74] and Reactome[75] databases to identify cellular/molecular pathways associated with the differentially translated genes.

Statistical analysis

GraphPad Prism v.9 software was used to analyze data. All data are presented as means ± s.e.m. An α=0.05 was used to determine statistical significance. Data analysis included unpaired Student's *t*-test

(two-tailed), one-way and two-way ANOVA, and repeated measures ANOVA, followed by between-group comparisons using Tukey's *post-hoc* test, as appropriate.

Acknowledgments: This study was supported by the Canadian Institutes of Health Research (PJT-162412) to A.K., FRN-154281 to J.S.M., and NIH NINDS grant NS065926 to T.J.P. A.K and C.G.G. were supported by General Secretariat for Research and Innovation Greece T12EPA5-00024 (C.G.G.), ERA-NET Neuron Sensory disorders project TRANSMECH. K.C.L. was supported by a Louise and Alan Edwards Foundation PhD fellowship.

Author contributions: K.C.L., S.U., J.S.M., and A.K. conceived the project, designed experiments, and supervised the research. K.C.L. performed immunohistochemistry and biochemistry analyses, surgeries, i.c.v. injections and mouse colony management. C.W., W.C., M.H. and N.B. assisted with behavioral experiments. S.U., M.A., M.P., L. D., S.M.J., Y.A., N.S. and C.G.G. performed Ribo-seq. D.T.F., N.I., K.M., and T.J.P assisted with TRAP analysis. N.G. performed electrophysiological experiments. HTZ and BF generated ASOs. F.B. and N.S. helped with data analysis and interpretation. K.C.L., J.S.M., and A.K. wrote the manuscript, with input from all authors.

Declaration of Interests: Hien T. Zhao and Bethany Fitzsimmons are full-time employees and shareholders of Ionis Pharmaceutical, Inc. Other authors declare no competing interests.

Materials Availability

This study did not generate new unique reagents.

Data Availability

Sequencing data generated in this study have been deposited in the Gene Expression Omnibus under the accession GSE265957.

References:

1. Finnerup, N.B., Kuner, R., and Jensen, T.S. (2021). Neuropathic Pain: From Mechanisms to Treatment. Physiol Rev *101*, 259-301. 10.1152/physrev.00045.2019.
2. Colloca, L., Ludman, T., Bouhassira, D., Baron, R., Dickenson, A.H., Yarnitsky, D., Freeman, R., Truini, A., Attal, N., Finnerup, N.B., et al. (2017). Neuropathic pain. Nat Rev Dis Primers *3*, 17002. 10.1038/nrdp.2017.2.

3. Costigan, M., Scholz, J., and Woolf, C.J. (2009). Neuropathic pain: a maladaptive response of the nervous system to damage. Annu Rev Neurosci *32*, 1-32. 10.1146/annurev.neuro.051508.135531.
4. Chen, G., Zhang, Y.Q., Qadri, Y.J., Serhan, C.N., and Ji, R.R. (2018). Microglia in Pain: Detrimental and Protective Roles in Pathogenesis and Resolution of Pain. Neuron *100*, 1292-1311. 10.1016/j.neuron.2018.11.009.
5. Peirs, C., and Seal, R.P. (2016). Neural circuits for pain: Recent advances and current views. Science *354*, 578-584. 10.1126/science.aaf8933.
6. Peirs, C., Williams, S.G., Zhao, X., Arokiaraj, C.M., Ferreira, D.W., Noh, M.C., Smith, K.M., Halder, P., Corrigan, K.A., Gedeon, J.Y., et al. (2021). Mechanical Allodynia Circuitry in the Dorsal Horn Is Defined by the Nature of the Injury. Neuron *109*, 73-90 e77. 10.1016/j.neuron.2020.10.027.
7. LaCroix-Fralish, M.L., Austin, J.S., Zheng, F.Y., Levitin, D.J., and Mogil, J.S. (2011). Patterns of pain: meta-analysis of microarray studies of pain. Pain *152*, 1888-1898. 10.1016/j.pain.2011.04.014.
8. Ray, P.R., Shiers, S., Caruso, J.P., Tavares-Ferreira, D., Sankaranarayanan, I., Uhelski, M.L., Li, Y., North, R.Y., Tatsui, C., Dussor, G., et al. (2023). RNA profiling of human dorsal root ganglia reveals sex differences in mechanisms promoting neuropathic pain. Brain *146*, 749-766. 10.1093/brain/awac266.
9. North, R.Y., Li, Y., Ray, P., Rhines, L.D., Tatsui, C.E., Rao, G., Johansson, C.A., Zhang, H., Kim, Y.H., Zhang, B., et al. (2019). Electrophysiological and transcriptomic correlates of neuropathic pain in human dorsal root ganglion neurons. Brain *142*, 1215-1226. 10.1093/brain/awz063.
10. Ghazisaeidi, S., Muley, M.M., Tu, Y., Finn, D.P., Kolahdouzan, M., Pitcher, G.M., Kim, D., Sengar, A.S., Ramani, A.K., Brudno, M., and Salter, M.W. (2023). Conserved transcriptional programming across sex and species after peripheral nerve injury predicts treatments for neuropathic pain. Br J Pharmacol *180*, 2822-2836. 10.1111/bph.16168.
11. Barry, A.M., Zhao, N., Yang, X., Bennett, D.L., and Baskozos, G. (2023). Deep RNA-seq of male and female murine sensory neuron subtypes after nerve injury. Pain *164*, 2196-2215. 10.1097/j.pain.0000000000002934.
12. Uttam, S., Wong, C., Amorim, I.S., Jafarnejad, S.M., Tansley, S.N., Yang, J., Prager-Khoutorsky, M., Mogil, J.S., Gkogkas, C.G., and Khoutorsky, A. (2018). Translational profiling of dorsal root ganglia and spinal cord in a mouse model of neuropathic pain. Neurobiol Pain *4*, 35-44. 10.1016/j.ynpai.2018.04.001.
13. Megat, S., Ray, P.R., Moy, J.K., Lou, T.F., Barragan-Iglesias, P., Li, Y., Pradhan, G., Wanghzou, A., Ahmad, A., Burton, M.D., et al. (2019). Nociceptor Translational Profiling Reveals the Ragulator-Rag GTPase Complex as a Critical Generator of Neuropathic Pain. J Neurosci *39*, 393-411. 10.1523/JNEUROSCI.2661-18.2018.
14. Geranton, S.M., Jimenez-Diaz, L., Torsney, C., Tochiki, K.K., Stuart, S.A., Leith, J.L., Lumb, B.M., and Hunt, S.P. (2009). A rapamycin-sensitive signaling pathway is essential for the full expression of persistent pain states. J Neurosci *29*, 15017-15027. 10.1523/JNEUROSCI.3451-09.2009.
15. Taniguchi, Y., Choi, P.J., Li, G.W., Chen, H., Babu, M., Hearn, J., Emili, A., and Xie, X.S. (2010). Quantifying E. coli proteome and transcriptome with single-molecule sensitivity in single cells. Science *329*, 533-538. 10.1126/science.1188308.
16. Schwanhausser, B., Busse, D., Li, N., Dittmar, G., Schuchhardt, J., Wolf, J., Chen, W., and Selbach, M. (2011). Global quantification of mammalian gene expression control. Nature *473*, 337-342. 10.1038/nature10098.
17. Bourke, A.M., Schwarz, A., and Schuman, E.M. (2023). De-centralizing the Central Dogma: mRNA translation in space and time. Mol Cell *83*, 452-468. 10.1016/j.molcel.2022.12.030.
18. Khoutorsky, A., and Price, T.J. (2018). Translational Control Mechanisms in Persistent Pain. Trends Neurosci *41*, 100-114. 10.1016/j.tins.2017.11.006.
19. Ingolia, N.T., Brar, G.A., Rouskin, S., McGeachy, A.M., and Weissman, J.S. (2012). The ribosome profiling strategy for monitoring translation in vivo by deep sequencing of ribosome-protected mRNA fragments. Nat Protoc *7*, 1534-1550. 10.1038/nprot.2012.086.

20. Heiman, M., Kulicke, R., Fenster, R.J., Greengard, P., and Heintz, N. (2014). Cell type-specific mRNA purification by translating ribosome affinity purification (TRAP). Nat Protoc *9*, 1282-1291. 10.1038/nprot.2014.085.
21. Decosterd, I., and Woolf, C.J. (2000). Spared nerve injury: an animal model of persistent peripheral neuropathic pain. Pain *87*, 149-158. 10.1016/S0304-3959(00)00276-1.
22. Millecamps, M., Sotocinal, S.G., Austin, J.S., Stone, L.S., and Mogil, J.S. (2023). Sex-specific effects of neuropathic pain on long-term pain behavior and mortality in mice. Pain *164*, 577-586. 10.1097/j.pain.0000000000002742.
23. Gingras, A.C., Raught, B., Gygi, S.P., Niedzwiecka, A., Miron, M., Burley, S.K., Polakiewicz, R.D., Wyslouch-Cieszynska, A., Aebersold, R., and Sonenberg, N. (2001). Hierarchical phosphorylation of the translation inhibitor 4E-BP1. Genes Dev *15*, 2852-2864. 10.1101/gad.912401.
24. Tahmasebi, S., Khoutorsky, A., Mathews, M.B., and Sonenberg, N. (2018). Translation deregulation in human disease. Nat Rev Mol Cell Biol *19*, 791-807. 10.1038/s41580-018-0034-x.
25. Ji, R.R., Gereau, R.W.t., Malcangio, M., and Strichartz, G.R. (2009). MAP kinase and pain. Brain Res Rev *60*, 135-148. 10.1016/j.brainresrev.2008.12.011.
26. Melemedjian, O.K., and Khoutorsky, A. (2015). Translational control of chronic pain. Prog Mol Biol Transl Sci *131*, 185-213. 10.1016/bs.pmbts.2014.11.006.
27. Truitt, M.L., Conn, C.S., Shi, Z., Pang, X., Tokuyasu, T., Coady, A.M., Seo, Y., Barna, M., and Ruggero, D. (2015). Differential Requirements for eIF4E Dose in Normal Development and Cancer. Cell *162*, 59-71. 10.1016/j.cell.2015.05.049.
28. Gkogkas, C.G., Khoutorsky, A., Ran, I., Rampakakis, E., Nevarko, T., Weatherill, D.B., Vasuta, C., Yee, S., Truitt, M., Dallaire, P., et al. (2013). Autism-related deficits via dysregulated eIF4E-dependent translational control. Nature *493*, 371-377. 10.1038/nature11628.
29. Santini, E., Huynh, T.N., MacAskill, A.F., Carter, A.G., Pierre, P., Ruggero, D., Kaphzan, H., and Klann, E. (2013). Exaggerated translation causes synaptic and behavioural aberrations associated with autism. Nature *493*, 411-415. 10.1038/nature11782.
30. Mohan, A., Fitzsimmons, B., Zhao, H.T., Jiang, Y., Mazur, C., Swayze, E.E., and Kordasiewicz, H.B. (2018). Antisense oligonucleotides selectively suppress target RNA in nociceptive neurons of the pain system and can ameliorate mechanical pain. Pain *159*, 139-149. 10.1097/j.pain.0000000000001074.
31. Hooshmandi, M., Wong, C., Lister, K.C., Brown, N., Cai, W., Ho-Tieng, D., Stecum, P., Backman, T., Kostantin, E., and Khoutorsky, A. (2024). Protocol for measuring protein synthesis in specific cell types in the mouse brain using in vivo non-canonical amino acid tagging. STAR Protoc *5*, 102775. 10.1016/j.xpro.2023.102775.
32. Dieterich, D.C., Hodas, J.J., Gouzer, G., Shadrin, I.Y., Ngo, J.T., Triller, A., Tirrell, D.A., and Schuman, E.M. (2010). In situ visualization and dynamics of newly synthesized proteins in rat hippocampal neurons. Nat Neurosci *13*, 897-905. 10.1038/nn.2580.
33. Barik, A., Sathyamurthy, A., Thompson, J., Seltzer, M., Levine, A., and Chesler, A. (2021). A spinoparabrachial circuit defined by Tacr1 expression drives pain. Elife *10*. 10.7554/eLife.61135.
34. Huang, T., Lin, S.H., Malewicz, N.M., Zhang, Y., Zhang, Y., Goulding, M., LaMotte, R.H., and Ma, Q. (2019). Identifying the pathways required for coping behaviours associated with sustained pain. Nature *565*, 86-90. 10.1038/s41586-018-0793-8.
35. Todd, A.J. (2010). Neuronal circuitry for pain processing in the dorsal horn. Nat Rev Neurosci *11*, 823-836. 10.1038/nrn2947.
36. Peirs, C., Dallel, R., and Todd, A.J. (2020). Recent advances in our understanding of the organization of dorsal horn neuron populations and their contribution to cutaneous mechanical allodynia. J Neural Transm (Vienna) *127*, 505-525. 10.1007/s00702-020-02159-1.
37. Khoutorsky, A., Bonin, R.P., Sorge, R.E., Gkogkas, C.G., Pawlowski, S.A., Jafarnejad, S.M., Pitcher, M.H., Alain, T., Perez-Sanchez, J., Salter, E.W., et al. (2015). Translational control of nociception via 4E-binding protein 1. Elife *4*. 10.7554/eLife.12002.

38. Petitjean, H., Pawlowski, S.A., Fraine, S.L., Sharif, B., Hamad, D., Fatima, T., Berg, J., Brown, C.M., Jan, L.Y., Ribeiro-da-Silva, A., et al. (2015). Dorsal Horn Parvalbumin Neurons Are Gate-Keepers of Touch-Evoked Pain after Nerve Injury. Cell Rep *13*, 1246-1257. 10.1016/j.celrep.2015.09.080.
39. Boyle, K.A., Gradwell, M.A., Yasaka, T., Dickie, A.C., Polgar, E., Ganley, R.P., Orr, D.P.H., Watanabe, M., Abraira, V.E., Kuehn, E.D., et al. (2019). Defining a Spinal Microcircuit that Gates Myelinated Afferent Input: Implications for Tactile Allodynia. Cell Rep *28*, 526-540 e526. 10.1016/j.celrep.2019.06.040.
40. Cao, B., Scherrer, G., and Chen, L. (2022). Spinal cord retinoic acid receptor signaling gates mechanical hypersensitivity in neuropathic pain. Neuron *110*, 4108-4124 e4106. 10.1016/j.neuron.2022.09.027.
41. Gangadharan, V., Zheng, H., Taberner, F.J., Landry, J., Nees, T.A., Pistolic, J., Agarwal, N., Mannich, D., Benes, V., Helmstaedter, M., et al. (2022). Neuropathic pain caused by miswiring and abnormal end organ targeting. Nature *606*, 137-145. 10.1038/s41586-022-04777-z.
42. Muralidharan, A., Sotocinal, S.G., Yousefpour, N., Akkurt, N., Lima, L.V., Tansley, S., Parisien, M., Wang, C., Austin, J.S., Ham, B., et al. (2022). Long-term male-specific chronic pain via telomere- and p53-mediated spinal cord cellular senescence. J Clin Invest *132*. 10.1172/JCI151817.
43. Pokhilko, A., Nash, A., and Cader, M.Z. (2020). Common transcriptional signatures of neuropathic pain. Pain *161*, 1542-1554. 10.1097/j.pain.0000000000001847.
44. Parisien, M., Samoshkin, A., Tansley, S.N., Piltonen, M.H., Martin, L.J., El-Hachem, N., Dagostino, C., Allegri, M., Mogil, J.S., Khoutorsky, A., and Diatchenko, L. (2019). Genetic pathway analysis reveals a major role for extracellular matrix organization in inflammatory and neuropathic pain. Pain *160*, 932-944. 10.1097/j.pain.0000000000001471.
45. Renthal, W., Tochitsky, I., Yang, L., Cheng, Y.C., Li, E., Kawaguchi, R., Geschwind, D.H., and Woolf, C.J. (2020). Transcriptional Reprogramming of Distinct Peripheral Sensory Neuron Subtypes after Axonal Injury. Neuron *108*, 128-144 e129. 10.1016/j.neuron.2020.07.026.
46. Coull, J.A., Boudreau, D., Bachand, K., Prescott, S.A., Nault, F., Sik, A., De Koninck, P., and De Koninck, Y. (2003). Trans-synaptic shift in anion gradient in spinal lamina I neurons as a mechanism of neuropathic pain. Nature *424*, 938-942. 10.1038/nature01868.
47. Coull, J.A., Beggs, S., Boudreau, D., Boivin, D., Tsuda, M., Inoue, K., Gravel, C., Salter, M.W., and De Koninck, Y. (2005). BDNF from microglia causes the shift in neuronal anion gradient underlying neuropathic pain. Nature *438*, 1017-1021. 10.1038/nature04223.
48. Yousefpour, N., Locke, S., Deamond, H., Wang, C., Marques, L., St-Louis, M., Ouellette, J., Khoutorsky, A., De Koninck, Y., and Ribeiro-da-Silva, A. (2023). Time-dependent and selective microglia-mediated removal of spinal synapses in neuropathic pain. Cell Rep *42*, 112010. 10.1016/j.celrep.2023.112010.
49. Kambrun, C., Roca-Lapirot, O., Salio, C., Landry, M., Moqrich, A., and Le Feuvre, Y. (2018). TAFA4 Reverses Mechanical Allodynia through Activation of GABAergic Transmission and Microglial Process Retraction. Cell Rep *22*, 2886-2897. 10.1016/j.celrep.2018.02.068.
50. Tansley, S., Gu, N., Guzman, A.U., Cai, W., Wong, C., Lister, K.C., Munoz-Pino, E., Yousefpour, N., Roome, R.B., Heal, J., et al. (2022). Microglia-mediated degradation of perineuronal nets promotes pain. Science *377*, 80-86. 10.1126/science.abl6773.
51. Yousuf, M.S., Shiers, S.I., Sahn, J.J., and Price, T.J. (2021). Pharmacological Manipulation of Translation as a Therapeutic Target for Chronic Pain. Pharmacol Rev *73*, 59-88. 10.1124/pharmrev.120.000030.
52. Price, T.J., Rashid, M.H., Millecamps, M., Sanoja, R., Entrena, J.M., and Cervero, F. (2007). Decreased nociceptive sensitization in mice lacking the fragile X mental retardation protein: role of mGluR1/5 and mTOR. J Neurosci *27*, 13958-13967. 10.1523/JNEUROSCI.4383-07.2007.
53. Xu, Q., Fitzsimmons, B., Steinauer, J., O'Neill, A., Newton, A.C., Hua, X.Y., and Yaksh, T.L. (2011). Spinal phosphinositide 3-kinase-Akt-mammalian target of rapamycin signaling cascades in inflammation-induced hyperalgesia. J Neurosci *31*, 2113-2124. 10.1523/JNEUROSCI.2139-10.2011.
54. Asante, C.O., Wallace, V.C., and Dickenson, A.H. (2009). Formalin-induced behavioural hypersensitivity and neuronal hyperexcitability are mediated by rapid protein synthesis at the spinal level. Mol Pain *5*, 27. 10.1186/1744-8069-5-27.

55. Liao, M.F., Lu, K.T., Hsu, J.L., Lee, C.H., Cheng, M.Y., and Ro, L.S. (2022). The Role of Autophagy and Apoptosis in Neuropathic Pain Formation. Int J Mol Sci *23*. 10.3390/ijms23052685.
56. Miller, Y.I., Navia-Pelaez, J.M., Corr, M., and Yaksh, T.L. (2020). Lipid rafts in glial cells: role in neuroinflammation and pain processing. J Lipid Res *61*, 655-666. 10.1194/jlr.TR119000468.
57. Roh, J., Go, E.J., Park, J.W., Kim, Y.H., and Park, C.K. (2020). Resolvins: Potent Pain Inhibiting Lipid Mediators via Transient Receptor Potential Regulation. Front Cell Dev Biol *8*, 584206. 10.3389/fcell.2020.584206.
58. Silva Santos Ribeiro, P., Willemen, H., and Eijkelkamp, N. (2022). Mitochondria and sensory processing in inflammatory and neuropathic pain. Front Pain Res (Lausanne) *3*, 1013577. 10.3389/fpain.2022.1013577.
59. Xiao, Y., Hsiao, T.H., Suresh, U., Chen, H.I., Wu, X., Wolf, S.E., and Chen, Y. (2014). A novel significance score for gene selection and ranking. Bioinformatics *30*, 801-807. 10.1093/bioinformatics/btr671.
60. Aguilar-Valles, A., De Gregorio, D., Matta-Camacho, E., Eslamizade, M.J., Khlaifia, A., Skaleka, A., Lopez-Canul, M., Torres-Berrio, A., Bermudez, S., Rurak, G.M., et al. (2021). Antidepressant actions of ketamine engage cell-specific translation via eIF4E. Nature *590*, 315-319. 10.1038/s41586-020-03047-0.
61. Sanz, E., Yang, L., Su, T., Morris, D.R., McKnight, G.S., and Amieux, P.S. (2009). Cell-type-specific isolation of ribosome-associated mRNA from complex tissues. Proc Natl Acad Sci U S A *106*, 13939-13944. 10.1073/pnas.0907143106.
62. Dobin, A., Davis, C.A., Schlesinger, F., Drenkow, J., Zaleski, C., Jha, S., Batut, P., Chaisson, M., and Gingeras, T.R. (2013). STAR: ultrafast universal RNA-seq aligner. Bioinformatics *29*, 15-21. 10.1093/bioinformatics/bts635.
63. Tarasov, A., Vilella, A.J., Cuppen, E., Nijman, I.J., and Prins, P. (2015). Sambamba: fast processing of NGS alignment formats. Bioinformatics *31*, 2032-2034. 10.1093/bioinformatics/btv098.
64. Pertea, M., Pertea, G.M., Antonescu, C.M., Chang, T.C., Mendell, J.T., and Salzberg, S.L. (2015). StringTie enables improved reconstruction of a transcriptome from RNA-seq reads. Nat Biotechnol *33*, 290-295. 10.1038/nbt.3122.
65. Wong, C., Tavares-Ferreira, D., Thorn Perez, C., Sharif, B., Uttam, S., Amiri, M., Lister, K.C., Hooshmandi, M., Nguyen, V., Seguela, P., et al. (2023). 4E-BP1-dependent translation in nociceptors controls mechanical hypersensitivity via TRIM32/type I interferon signaling. Sci Adv *9*, eadh9603. 10.1126/sciadv.adh9603.
66. Tavares-Ferreira, D., Ray, P.R., Sankaranarayanan, I., Mejia, G.L., Wangzhou, A., Shiers, S., Uttarkar, R., Megat, S., Barragan-Iglesias, P., Dussor, G., et al. (2022). Sex Differences in Nociceptor Translatomes Contribute to Divergent Prostaglandin Signaling in Male and Female Mice. Biol Psychiatry *91*, 129-140. 10.1016/j.biopsych.2020.09.022.
67. Zhang, X.D., Marine, S.D., and Ferrer, M. (2009). Error rates and powers in genome-scale RNAi screens. J Biomol Screen *14*, 230-238. 10.1177/1087057109331475.
68. Chaplan, S.R., Bach, F.W., Pogrel, J.W., Chung, J.M., and Yaksh, T.L. (1994). Quantitative assessment of tactile allodynia in the rat paw. J Neurosci Methods *53*, 55-63. 10.1016/0165-0270(94)90144-9.
69. Langford, D.J., Bailey, A.L., Chanda, M.L., Clarke, S.E., Drummond, T.E., Echols, S., Glick, S., Ingrao, J., Klassen-Ross, T., Lacroix-Fralish, M.L., et al. (2010). Coding of facial expressions of pain in the laboratory mouse. Nat Methods *7*, 447-449. 10.1038/nmeth.1455.
70. Bailey, T.L., Johnson, J., Grant, C.E., and Noble, W.S. (2015). The MEME Suite. Nucleic Acids Res *43*, W39-49. 10.1093/nar/gkv416.
71. Bolger, A.M., Lohse, M., and Usadel, B. (2014). Trimmomatic: a flexible trimmer for Illumina sequence data. Bioinformatics *30*, 2114-2120. 10.1093/bioinformatics/btu170.
72. Xiao, Z., Zou, Q., Liu, Y., and Yang, X. (2016). Genome-wide assessment of differential translations with ribosome profiling data. Nat Commun *7*, 11194. 10.1038/ncomms11194.
73. Chen, E.Y., Tan, C.M., Kou, Y., Duan, Q., Wang, Z., Meirelles, G.V., Clark, N.R., and Ma'ayan, A. (2013). Enrichr: interactive and collaborative HTML5 gene list enrichment analysis tool. BMC Bioinformatics *14*, 128. 10.1186/1471-2105-14-128.

74. Kanehisa, M., Furumichi, M., Tanabe, M., Sato, Y., and Morishima, K. (2017). KEGG: new perspectives on genomes, pathways, diseases and drugs. Nucleic Acids Res *45*, D353-D361. 10.1093/nar/gkw1092.

75. Fabregat, A., Sidiropoulos, K., Viteri, G., Forner, O., Marin-Garcia, P., Arnau, V., D'Eustachio, P., Stein, L., and Hermjakob, H. (2017). Reactome pathway analysis: a high-performance in-memory approach. BMC Bioinformatics *18*, 142. 10.1186/s12859-017-1559-2.